Using an Empirical Model of Human Turning Motion to Aid Heading Estimation in a Personal Navigation System

A THESIS
SUBMITTED TO THE FACULTY OF THE GRADUATE SCHOOL
OF THE UNIVERSITY OF MINNESOTA
BY

Thomas Jakel

IN PARTIAL FULFILLMENT OF THE REQUIREMENTS
FOR THE DEGREE OF
MASTER OF SCIENCE

Demoz Gebre-Egziabher
December 30, 2013

Acknowledgments

There are far too many people to acknowledge for me to include a comprehensive list of the people that positively affected this work, so for those of you who may have been excluded I am sincerely sorry.

First and foremost, I would like to acknowledge my adviser, Demoz Gebre-Egziabher, for inspiring my interest in navigation, sensor fusion and estimation and for providing feedback on my work. His enthusiasm for navigation and sensor fusion is contagious and sparked the curiosity that lead to this work.

Next I would like to express my sincere gratitude to Adam Rozumalski and Michael Schwartz for assisting me in the James R. Gage Gait Analysis Lab and providing insight on performing gait analysis with the Vicon® Motion Capture System. Without you the reference system used to validate the results of this work would not have been possible.

I would also like to thank Chris Matthews and Ryan Kirker for their insight and discussions on their previous research that influenced the trajectory of this work.

To Suneil Sheikh and John Condon thank you for your help calibrating the Bluetooth IMUs. I look forward to future revisions of the research and inertial measurement units.

I am also obliged to Larry Vallot, Scott Snyder, and Richard Russell of Honeywell for mentoring me during the early stages of my career. Your mentoring has played a critical role in my technical development and your influences are evident in this work.

To Gary Balas, Paw Yew Chai, and Rohit Pandita, my former UAV Group colleagues, thank you for teaching me about systems engineering. The origin of this work comes from assignments given working on the IMU in the control and navigation system of the Ultrastick UAV.

I would like to offer my sincere thanks to Hamid Mokhtarzadeh and Adhika Lee for helping me revise my defense presentation and being available to bounce ideas off of.

Finally, I would like to thank the study participants who cannot be mentioned by name due but played a critical role in this work.

Dedication

This work is dedicated to my future wife, Olivia Jean Richardson, for giving me love and support required for me to complete my studies while working full time. Your patience and willingness to listen brighten my outlook and sharpen my mind.

I would also like to dedicate this work to my parents John and Deb Jakel for listening, answering, and encouraging my questions as an inquisitive child. Without your sacrifices I would not be who I am today.

Finally, I would like to dedicate this work to my Grandparents Lillian and Roger Van Natta who taught me to be patient, hardworking and humble.

Abstract

With the adoption of Global Navigation Satellite Systems in smart phones, soldier equipment, and emergency responder navigation systems users have realized the usefulness of low cost Personal Navigation Systems. The state-of-the-art Personal Navigation System is a unit that fuses information based on external references with a low cost IMU.

Due to the size, weight, power, and cost constraints imposed on a pedestrian navigation systems as well as current IMU performance limitations, the gyroscopes used to determine heading exhibit significant drift limiting the performance of the navigation system.

In this thesis biomechanical signals are used to predict the onset of pedestrian turning motion. Experimental data from eight subjects captured in a gait laboratory using a Vicon motion tracking unit is used for validation. The analysis of experimental data shows the heading computed by turn prediction augmented integration is more accurate than open loop gyro integration alone.

Contents

LIST OF TABLES

LIST OF FIGURES

1. Introduction

Personal navigation systems are devices carried or worn by individuals to provide an estimate of their navigation state vector. The navigation state vector consists of the user's position, velocity and attitude or a subset of these quantities. With the invention and public adoption of Global Navigation Satellite Systems (GNSS), low cost personal navigation systems have given individuals the ability to know their position to within meters provided they have access to the open sky. For personal navigation applications that require operation indoors or where the quality of the GNSS signal is degraded, however, an alternative means of navigation must be used. One such scenario is depicted in Figure 1 [11] which shows the case of a first-responder entering a building during an emergency. The first-responder starts navigating outside the building (point A) where GNSS signals are available. Upon entering the building (point B) the ability to navigate visually is lost perhaps due to smoke or fire. GNSS signals are also lost. From this point on until reaching the destination (point C) a non-GNSS navigation system must be used.

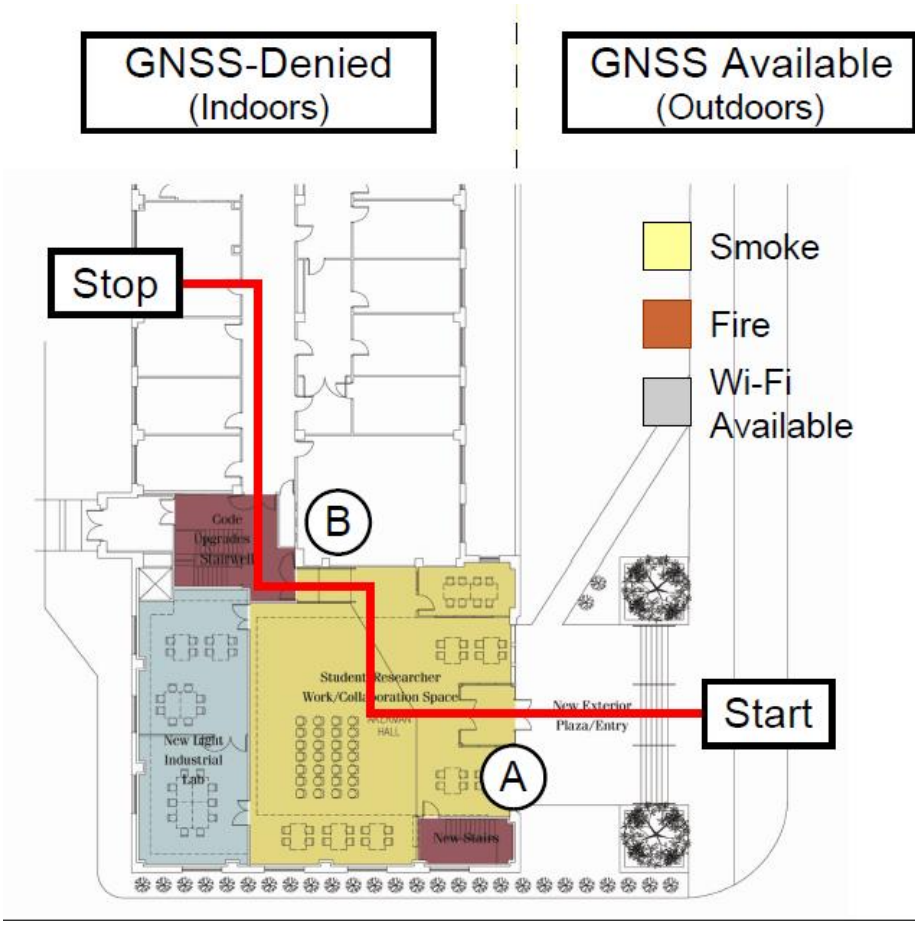

Figure 1-1. Scenario requiring non-GNSS indoor navigation capability (First responder navigation).

The challenge depicted in Figure 1 has been the impetus, in part, to develop methods that utilize alternate means of navigation to augment GNSS in personal navigation systems. Most of these systems identified as solution for this problem make use of low cost MEMS rate gyros and accelerometers integrated into an Inertial Measurement Unit (IMU). Their small size, weight and power consumption make IMU attractive for this application. The IMUs are used to implement a dead reckoning solution. This involves initializing the system from previous navigation state information when aiding information was available and numerically integrating the acceleration and angular rate measurements from the IMU to update the estimate of the navigation state vector. Because locating an IMU on the foot or the small of the back (lumbar region) results in a simpler and more secure installation, many of the IMU-based dead reckoning (DR) solutions for personal navigation tend to use this installation architecture.

Given the current state of the art low cost commercial grade IMU stand-alone dead reckoning is not possible because when the large sensor output errors are integrated numerically they lead to a significant accumulation of navigation error. To deal with this issue, numerous methods to aid the dead reckoning solution have been

proposed. These aiding methods include using zero velocity updates or ZUPTs for foot mounted IMUs [3]; using magnetometers to measure attitude relative to the earth's magnetic field [13]; using Wi-Fi or RFID signals for range measurements [7]; vision aiding [4]; stride length estimation using gait models [9]; and motion classification algorithms [10]. Each of these methods has merit, but also has drawbacks associated with its use. The work in this paper deals with improving the heading solution of systems which use foot-mounted IMUs aided by ZUPTs.

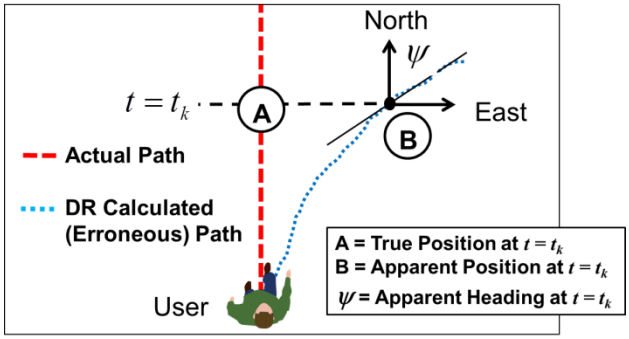

Figure 1-2. Actual heading change vs. erroneous (apparent) heading change.

1.1 MOTIVATION

Regardless of what part of the body the IMU is installed on or what aiding sensor is chosen most IMU-based systems make use of some form ZUPTs. This allows the DR system, without any additional sensors, to estimate velocity error directly. It also allows indirect estimation of roll and pitch errors which affect the resolution of the accelerometers' measurement of the gravity vector in the IMU frame. However these zero velocity updates do not allow the navigation system to observe any information about the rotation about the heading axis—the axis aligned with the gravity vector and perpendicular to the ground below the foot [3]. This leads to heading errors which grow over time. For example, a user walking in a straight line would observe that the DR system is indicating continuous heading change as shown in Figure 2 (i.e., the true heading should be zero in this case but the DR system computes a non-zero value which continues to grow with time). In order to improve the dead reckoning solution, more information about the heading error and heading change during walking motion is needed. Such a method would be complementary to the zero velocity update information.

In view of the discussion above, this paper attempts to answer the following question: In addition to the fact that the foot has a zero velocity at the end of each step (i.e. ZUPTs) are there other biomechanical signature of human gait that can be measured by IMUs and used to improve the accuracy of the DR heading estimate? As we will show in this paper, the answer to this question is "yes" these biomechanical signals of interest can be measured by the combination of a trunk (or lumbar) and foot mounted IMUs. It will be shown that

these biomechanical signatures are a reliable indicator that an individual has started or is ending a turn. When used in a DR system, these signatures would be used to distinguish apparent (or fictitious) heading changes caused by gyro and accelerometer errors from actual (physical) heading changes caused by a turn.

1.2 PRIOR ART

The method presented in this paper can be viewed as an extension and improvement of prior work described in [1], [2] and [3]. The work described in [3] uses a foot mounted IMU to mechanize a dead reckoning system in the form of an Inertial Navigation System (INS) aided by ZUPTs only. Since heading errors cannot arrest heading errors, use of a magnetometer triad is proposed as an aiding sensor. The drawback of magnetometers is that they are easily affected by proximity to magnetic fields due to current carrying wires or ferromagnetic materials—a rather typical occurrence indoors.

The work in [1] uses the gyros in a foot-mounted IMU to determine heading. During straight line walking, gyro outputs are passed through a low pass filter before they are used to determine heading. The low pass filter is used to separate actual heading changed (low frequency content signal) from apparent heading change due to gyro drift (higher frequency content signal). As noted in [1], this approach fails when the user makes sharp or abrupt heading changes when the true signal has higher frequency content than the apparent signal. Since sharp turns are common during indoor navigation, the approach proposed in [1] is limited to use outdoors during straight line walking.

The work in [2] proposes a waist mounted triad of accelerometers and single gyroscope to mechanize a dead reckoning system. The proposed approach uses the periodicity of trunk yaw as a biomechanical signature from which strides and turns can be identified. The drawback of this method is that an individual unique calibration is required and the accuracy of the system is dependent on the similarity between the calibration (one single 360° turn) and the future turns made by the user.

1.3 THESIS CONTRIBUTIONS

In response to the challenging problem described above the following are the contributions of this thesis:

- A method, algorithm and framework for pedestrian turn detection and heading error reduction of low cost trunk mounted inertial navigation systems
- A novel experiment to test the inertial navigation solution
- Statistics of critical turning indication parameters of 8 healthy subjects of varying heights, weights and sex

1.4 THESIS OUTLINE

- Chapter 2 lays the ground work for the theory of using a model of human motion to aid a pedestrian navigation system
- Chapter 3 describes the setup of the experiment used to test the algorithms developed to reduce heading error drift in the pedestrian navigation application, this also includes the data processing used to prepare the reference data to the experimental data
- Chapter 4 describes the algorithms run on the inertial data from the foot and trunk mounted sub-systems
- Chapter 5 describes the results of the algorithms used to navigate the foot and determine the heading of the torso, conclusions and future work are also discussed

2 Concept of Model Based Aiding for Pedestrian Navigation

2.1 BIOMECHANICS OF TURNING

Turning is defined as a reorientation of the body to achieve a new direction of travel. In human beings a large percentage of the mass is concentrated in the upper body which means that body reorientation will require reorientation of the trunk. The quantities of interest for this model of turning motion are quantities that predict the onset of turning and/or give a measure of the turning motion that has occurred.

Previous research in turning motion has shown that

1) In order to alter the direction of locomotion without stopping the change in direction has to be planned in the previous step [18].

2) During normal human gait, turning without stopping is the preferred method of direction change [17].

3) The human body can be modeled as a double pendulum with turning motion initiated by the upper body rotating about the frontal plane [17].

2.1.1 Kinetic Analysis

Kinetic analysis of the human body system undergoing turning motion suggests that in order for there to be an angular displacement about the vertical axis there must be moment about the vertical axis. Consider a person making a right turn just prior to body reorientation with the right foot just being picked up off the ground. For a turn to occur an external moment about the vertical axis must be provided by the left foot to satisfy the equation:

$$\alpha_{Body} = \sum \frac{M_{Left\ Foot}}{I_{Body/Foot}} \tag{2.1.1}$$

Over the course of the right foot swing phase the total angle change is given by:

$$\Delta\theta_{Body} = \omega_{Body,0}\left(t_1 - t_0\right) + \int_{t_o}^{t_1}\left(\int_{t_0}^{t_1}\left(\alpha_{Body}dt\right)\right)dt \tag{2.1.2}$$

The change in angle computed by equation (2.1.2) describes the bulk motion of the human body system but does not give any kinematic information on the individual limbs and joints that make up the body. This

kinematic information is essential since the personal navigation system tracks the kinematic information of a single limb or multiple limbs, not every limb in the human body.

There are two possible methods to obtain kinematic information about the individual limbs. The first is to track the transmission of moments through the joints, and the second is to directly observe the kinematic quantities of all limbs of interest during the turn. It is more practical to observe kinematic quantities directly than to calculate them by force-moment relations, therefore the approach of tracking limb motion is taken.

The kinematic quantities of human limbs turn during walking motion is described in [17]. This work showed that foot placement and trunk roll motion are the main controlling mechanisms behind turning motion of people. For a foot mounted pedestrian navigation system the interest is in quantities that provide information on the magnitude of reorientation of the foot. For the purpose of simplification the model here assumes turning to the left and right to be symmetrical and therefore the focus here is on a turn by a person to the right. The assumed turning motion takes place with a person walking along a straight line then making a turn to the right at a significant angle

2.1.2 Kinematic Analysis

The approach described in this thesis hinges on the assumption that observing the kinematic states of an individual's trunk and foot provides an unambiguous clue as to whether an individual is walking in a straight line or turning. Research about the way turning is executed by healthy individuals during walking motion has been performed by the neurological and medical community [16, 17, 18]. The literature in these domains illustrates that turning motion is most commonly performed without stopping and is a coordinated effort between the trunk and the lower body [17]. The kinematic parameters affected by turning motion are trunk roll, trunk yaw, foot stride length, and foot stride width [17].

For our purposes trunk roll and yaw will be defined as rotational misalignments between the orthogonal axes attached to the IMU located on the user's trunk (i.e trunk sensor axes) and the standard North-East-Down (NED) navigation frame whose origin is at the user's current location. We are assuming that the trunk sensor axes are aligned in such a way that the x-axis points, the z-axis points down and the y-axis completes the right-handed coordinate system. Trunk yaw (ψ_T) is the first rotation in a 3-2-1 Euler angle sequence that transforms the navigation frame into the sensor frame. Stated another way, it is a rotation about the vertical axis from the navigation frame to the sensor frame. Similarly, the trunk roll (ϕ_T) is the third rotation in the same 3-2-1 Euler angle sequence that transforms the navigation frame into the trunk sensor frame. The trunk roll and yaw angles are depicted in Figures 4(a) and 4(b), respectively.

The remaining two parameters of interest are related to the orientation of either foot. The first of these is the foot yaw angle (ψ_F) which is defined as the first Euler angle in a 3-2-1 sequence that rotates transforms the navigation frame into the foot-mounted IMU frame. The foot-mounted IMU's axes are aligned in such a way that the x-axis is point forward; the z-axis is pointing down and the y-axis complete s the right-handed coordinate system. The last of the kinematic parameters is stride width (denoted *SW*). It is defined as the perpendicular displacement of either the right or left foot relative to a straight line originating from the foot's position at the last step and drawn parallel to the direction of travel over the previous stride. Both the foot yaw and step width are shown graphically in **Figure 4-2**, respectively.

When an individual walks, trunk yaw, trunk roll, foot yaw and stride width are not constant but vary continuously. During straight line walking the *change* in these parameters from one step to the next can be described as a zero-mean, random process with a known variance. However, during a turn the random process which described the change in these parameters from step to step will exhibit a shift in mean, variance or both. Suppose we view the straight line walking and turning maneuvers as distinct random processes characterized by the distributions of $\Delta\psi_T$, $\Delta\phi_T$, $\Delta\psi_F$ and SW. Then identifying whether an individual is walking in a straight line or turning becomes a problem of determining a change in process. As such, we first need to determine the baseline statistics of $\Delta\psi_T, \Delta\phi_T$, $\Delta\psi_F$ and SW during straight line walking.

Baseline statistics for the four kinematic parameters was obtained from an experiment in which we instrumented subjects with sensors and measured the kinematic states of various limbs and body parts as they walked. The experiments were conducted in a hospital setting at the James R. Gage Center for Gait and Motion Analysis at the Gillette Healthcare [14]. The laboratory is equipped with a Vicon™ motion capture system [15] which uses an array of cameras to track the motion of markers placed on various parts of a subject's body. The experiment consisted of eight healthy participants (two female and six males ages twenty-two to thirty-eight) instrumented with five IMUs on their upper torso, lower torso, right thigh, right leg, and right foot. The details of the experimental set up and data processing will be discussed in more depth later in the paper. For now, however, we will just focus on the characterization of kinematics parameters obtained from these experiments.

Figure 2-1 and 4 show histograms of $\Delta\psi_T$ and $\Delta\phi_T$. The histograms were prepared using all the data from all the subjects in the experiment. Figure 2-1 shows a histogram of change in the trunk yaw angle during a stride for straight line walking. Even though we will discuss this histogram in more detail later, for now the key point to take away is that the torso's yaw angle is not a constant during straight line motion but varies.

Its variation can be characterized by a histogram (or, with sufficient data, a probability density function) with a distinct mean and variance. When a turn occurs, the mean and variance will change. The change is one of the signatures we exploit in the approach presented in this paper.

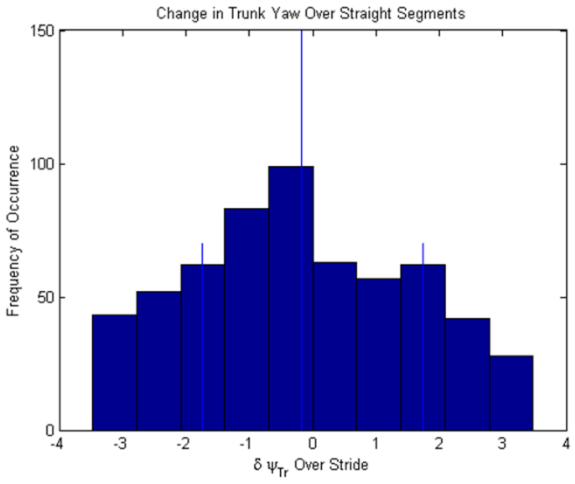

Figure 2-1 The change in trunk yaw over straight segments

Similarly, Figure 2-2 shows a histogram of change in the trunk roll angle over a stride for straight line walking. Once again, we have a distribution with a distinct mean and variance. Deviations from this (in a statistical sense) can be used a signature for a deviation from straight line walking.

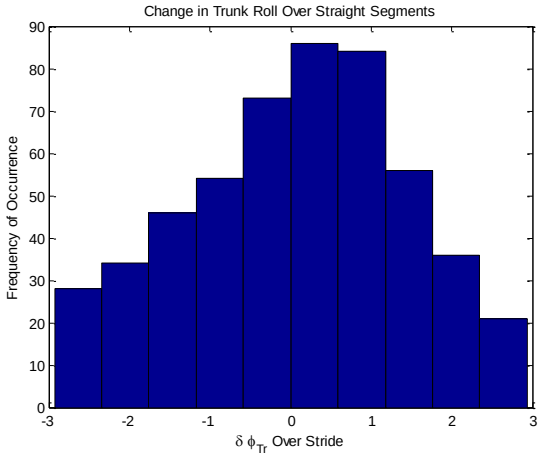

Figure 2-2 The change in trunk roll over straight segments

In the algorithm that will be described next we will use "hard" thresholds to determine when a deviation from straight line walking has occurred. Figure 6 and 7 will be used to establish the thresholds for $\Delta\psi_T$ and $\Delta\phi_T$. Thresholds for $\Delta\psi_F$ and SW will be discussed later.

Figures 6 and 7 provide the explanation we propose using four kinematic parameters to detect the occurrence of turns. Since these kinematic parameters are random variables, during straight line walking it is reasonable to expect that a single sample of a particular kinematic parameter can exceed the established threshold. To avoid declaring a turn (a false alarm) when a single parameter exceeds a threshold, we will use the more conservative approach of declaring a turn when two out of four parameters exceed the established thresholds. $\Delta\psi_T$ or $\Delta\phi_T$ alone cannot be used as the kinematic parameters or signatures for identifying a turn. This is because as shown in Figure 2-1 and Figure 2-2, $\Delta\psi_T$ and $\Delta\phi_T$ are random variables and taking a single sample of a random variable and attempting to determine whether that random variable came from a particular distribution is a less precise method of parameter estimation than observing the distribution through a separate but dependent variable.

2.2 SYSTEM CONCEPT

The dead reckoning approach for personal navigation described in this paper fuses the information from three information sources; an IMU-based sub-system installed on the foot of the user, an IMU-based sub-system on the trunk of the user and turn detection sub-system containing logic for determining deviation from straight line walking.

The foot mounted sub-system generates an estimate of the user's navigation state vector. It uses ZUPTs mitigate drift in the state vector estimate due to IMU errors. In addition, it generates estimates of $\Delta\psi_F$ and SW which is used by the turn detection sub-system. The trunk-mounted system tracks the attitude of the user's trunk from which it generates estimates of $\Delta\psi_T$ and $\Delta\phi_T$. The estimates of $\Delta\psi_T$ and $\Delta\phi_T$ are used by the turn detection sub-system. The turn detection sub-system uses the estimate of $\Delta\psi_T$, $\Delta\phi_T$, $\Delta\psi_F$ and SW provided by the other two sub-system to decide whether deviation from straight line walking has occurred. In what follows we will described the algorithms running in each sub-system conceptually.

2.2.1 Foot Mounted Sub-System

The foot-mounted system is essentially a ZUPT-aided inertial navigation system. An Extended Kalman Filter (EKF) is used to fuse the IMU outputs with ZUPTs. The system used in this work is essentially the same as the one described in [3] with one major difference. The difference is in how the EKF estimates yaw. If the turn detection sub-system indicates that the user is walking in a straight line, then it interprets any consistent change in heading as being apparent heading change due to gyro drift. Thus, it keeps the heading change to zero and uses this information as a pseudo-measurement which can be used to estimate the gyro bias.

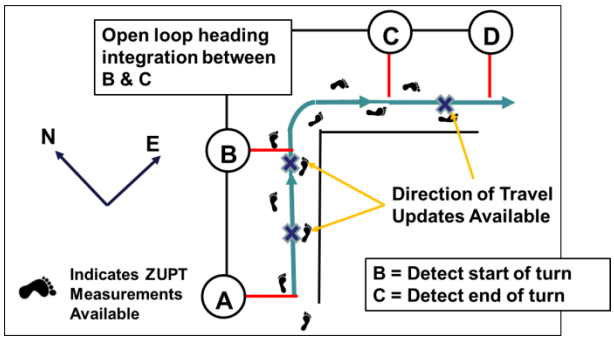

Figure 2-3. Graphic depiction of system operation

Figure 5 graphically describes the system operation. In the figure, the user starts walking in a straight line (segment AB), makes a 90 degree turn to the right (segment BC) and continues to walk in straight line (segment CD). Along segment AB the turn detection logic would indicate straight line walking. Therefore, any heading change along this segment will be interpreted as being due to IMU errors. At point B, the turn detection logic indicates deviation from straight line walking. This results in the "unclamping" of the change in yaw estimate by the foot-mounted system (i.e. open loop integration of the IMU). Once the end of the turn is detected, the foot-mounted system "clamps" the expected change in yaw to be zero.

2.2.2 Trunk Mounted Sub-System

The trunk mounted sub-system determines the attitude of the trunk. The process for estimation of trunk attitude is shown in Figure **2-4**. The process starts by determination of initial attitude of the trunk. The changes in attitude relative to the initial attitude is determined through the integration of the trunk mounted angular rate sensors until the end of a stride is detected. Once the stride end is detected if the motion is determined to not be a turn, then the attitude information from the previous stride is used to remove any drift caused by integration of gyroscope errors.

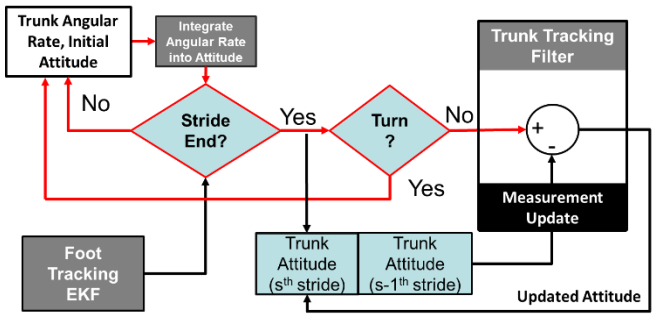

Figure 2-4. The process of estimating trunk attitude

To form the attitude measurement for the current right foot contact, which is effectively used to constrain the motion of the trunk to a straight line path, the initial attitude must be known. The initial attitude of the

trunk is assumed to be known before the user enters a GNSS-denied area. At the start, this attitude is used to initialize the trunk sub-system. For the experiment used to analyze turning motion the initial orientation of the IMU is measured by the Vicon® system.

3 Experimental Analysis

The purpose of the experiment conducted under this research is to analyze the use of a human turning motion model used to aid Strapdown Navigation. Analysis of the human turning model described in section 2.1.2 and previous experiments suggest that trunk roll angle, trunk yaw angle, stride length deviation from nominal stride, angle change of the foot over a stride and magnitude of foot placement perpendicular to the direction of stride are indicators of the onset of turning motion (Patla, Adkin and and Ballard). A Vicon® Motion capture system is used as a reference for Inertial Measurement Units (IMUs), which are more typically used for Strapdown Inertial Navigation and pedestrian motion tracking.

3.1 EXPERIMENT SETUP

The experiment participants are eight healthy adults (6 male and 2 female) weighing between 50 and 90 kg (110 – 200 lb) and measuring in height between 165 and 190 cm (5’5’’ – 6’3’’). By having variability in the height, weight and sex of the subjects selected it allows for analysis of how much or little effect each of the varied factors have on the parameters of interest during turning motion. For the purpose of aiding navigation the interest is in parameters that do not vary across subjects or can easily be calibrated during operation of a navigation system with GNSS or other aiding sensors.

Due to the use of a Vicon® Motion Capture System for tracking of limb motion the area used for the experiment is confined to a small 10 meter by 5 meter room. This is considered acceptable since the turning motion of interest is indoor or confined space turning motion. To mimic natural walking through hallways each subject is asked to walk five repetitions of four separate trajectories at both a fast and a slow pace. These trajectories are straight line walking, walking with a 45° turn, walking with a 90° turn, and walking with periodic turning motion. Prior to beginning each of these trajectories the participant is asked to stand as still as possible to allow for initialization of the navigation algorithms.

Having the subjects walk in a straight line and then turn around as shown in *Figure 3-1* is meant to be a control trajectory intended to determine the capability of turning detection to identify segments of motion that are nominally straight.

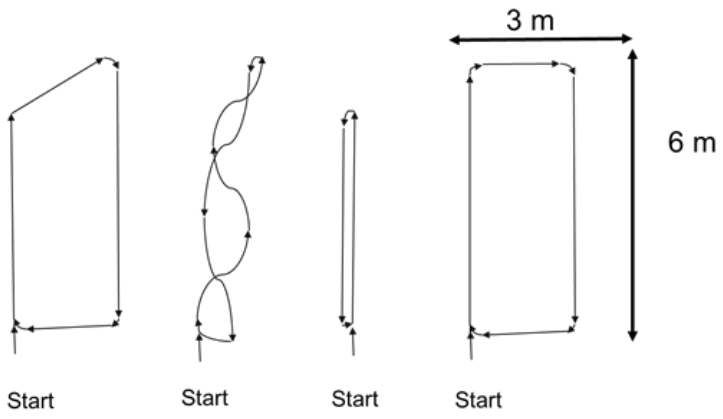

Figure 3-1 The paths walked by the participants

3.1.1 Vicon® Measurement System Setup

The Vicon® Measurement system is a set of infrared cameras and reflector dots that provides the user with the position of reflector dots relative to a point in the room. The particular Vicon setup being used for this experiment is the Vicon System at the Gait and Motion Analysis Center of Gillette Children's Hospital which is a system with accuracies around 2 mm. (Rozumalski). Prior to having participants complete the walking trajectories specified they are instrumented with a Vicon® reflector dot in every place where it is desired that there be a position measurement. In this experiment the upper torso, lower torso, right thigh, left thigh, right shin, left shin, right foot, and left foot are tracked with Vicon® markers. Each of these limbs are instrumented up with three Vicon® markers to allow for a reconstruction of the limb's position and orientation as described in Section 3.3.3 step 2. The instrumentation of the subject is as illustrated in Figure 3-2.

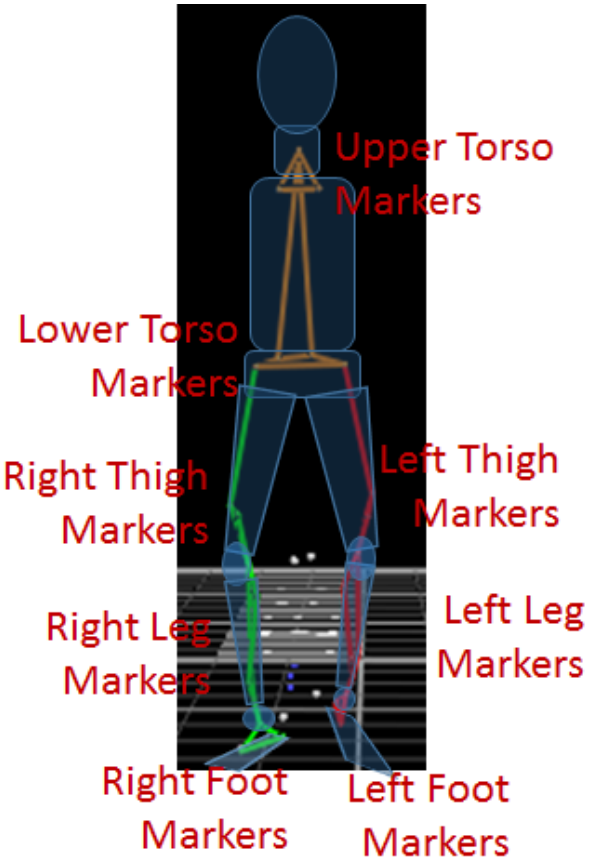

Figure 3-2 The Vicon instrumentation of the test participant

3.1.2 Inertial Measurement Unit Setup

A standard Inertial Measurement Unit consists of three accelerometers, which measure specific force, and three gyroscopes, which measure angular rate, with the measurement axis of the accelerometers the gyroscopes aligned. Each of these sets of accelerometer/gyroscope pairs is placed perpendicular to the remaining two sets in an axis set that follows a right handed convention; this allows for a measurement of specific force and angular rate in three independent directions as shown in

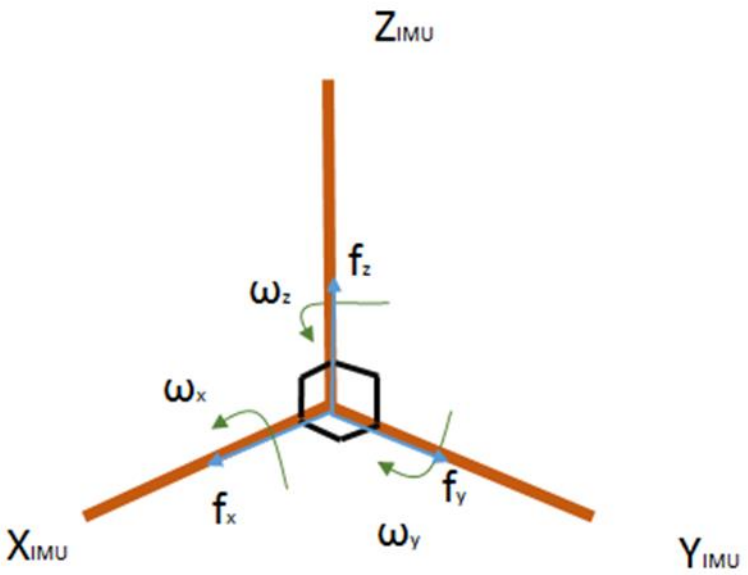

Figure 3-3 The nominal axes for IMU Measurements

The IMU used in this experiment is a custom built IMU from Advanced Medical Electronics that transmits A/D converted counts of measured voltages proportional to angular rate and specific force over Bluetooth to a recording PC that stores the data (Procedure described in section 8.1) for use in the IMU calibration routines described in section 3.3.1. The IMU and Bluetooth transmitter are packaged in a 1.5''x 1.5'' plastic mounting case shown in Figure 3-4 with handles that are used to secure the case to the participant by Velcro strap.

Figure 3-4 The Bluetooth IMU used for the experiments with a quarter for size reference

Even after calibration the IMU quality is consumer grade unit with accelerometer bias and bias stability quantities on the order of 0.2 m/s^2 and gyro bias and bias stability quantities on the order of 0.5°/s. These residual error quantities are discussed further in sections 4 and 5.2.3. IMUs with sensors of this quality (shown in **Table 1: IMU Parameters Used in the Experiment**) are readily available from vendors such as

Analog Devices, however the Bluetooth data transmission feature is critical for this experiment since it made the instrumentation of the IMUs on the experiment participants simple and there was no wiring to interfere with the natural motion of the subjects.

Table 1: IMU Parameters Used in the Experiment

IMU Parameter Description	Value
Correlation Time Constant of Gyro(τ_g)	300 (sec)
Stdv of Gyro Markov Bias ($\sigma_{\mu g}$)	0.3 (deg/s)
Stdv of Gyro Wide Band Noise(σ_{wg})	0.1 (deg/s)
Correlation Time Constant of Acc (τ_a)	500 (sec)
Stdv of Acc Markov Bias ($\sigma_{\mu a}$)	0.01 g (m/s/s)
Stdv of Acc Wide Band Noise (σ_{wa})	0.005 g (m/s/s)

The particular version of the IMU software used in this experiment have a bug that occasionally cause the IMU to drop Bluetooth transmission; this was a cause of data sets that do not contain a particular IMU.

3.2 FRAME DEFINITION

Navigation is the ability to describe an object's position, orientation and derivatives of these quantities relative to some reference frame. This frame should be chosen for user convenience to allow physical understanding of the navigation solution presented. In this experiment there are a number of reference frames presented that are convenient to describe certain measured quantities in. For this experiment the frames used are the IMU Body Frames, Vicon Body Frames, Vicon Global Frame and North, East, Down (NED) Frame.

The Vicon Global Frame is defined by the Vicon® measurement software as axes fixed in orientation and location relative to the surface of the earth. The position measurements of the Vicon® Markers are given in this frame. The Vicon® Global Frame Z-axis points up toward the ceiling of the lab and the X-axis points along the direction of the person's initial steps with the Y-axis being defined as the cross product of the Z and X axes. The orientation of the Vicon Global Frame relative to the NED axis is shown in Figure 3-7.

The NED coordinate frame consists of the North and East axes which are on a plane tangent to the earth's surface at that point. The North axis points toward the earth's true North Pole and the East axis is the vector perpendicular to the North axis on the tangent plane. The down axis is the axis perpendicular to both the North and East axes pointing toward the center of the earth. This is the coordinate frame end

navigation quantities are described in. Its orientation relative to the Vicon Global Frame is shown in Figure 3-6. The IMU Body Frame is fixed relative to the Inertial Measurement Unit. This is the coordinate frame that the triad of accelerometers and triad of gyroscopes output data in. As shown in Figure 3-5 the X axis points out the connectors of the IMU, the Z axis points toward the flat mounting surface, and the Y axis points toward the right mounting strap as viewed from above (when the label is showing)

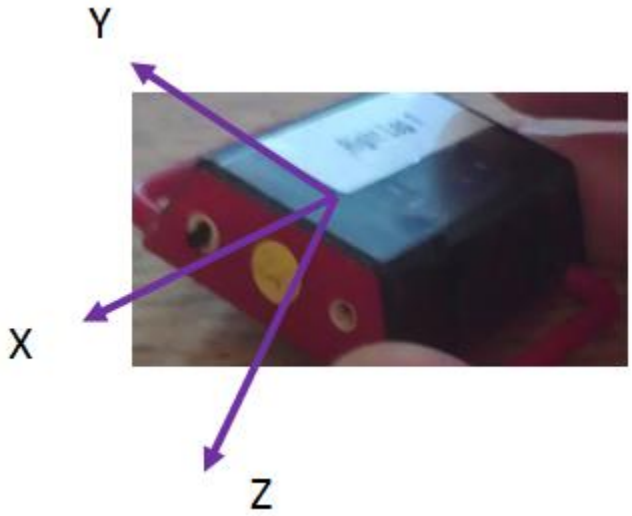

Figure 3-5 The Inertial Measurement Unit Body Frame shown overlaid on the Right Leg IMU

Due to mounting constraints each IMU mounted on limb has a different orientation relative to the NED coordinate frame at the beginning of the trial, however for all eight participants the IMU orientation on a given limb is approximately the same to mounting precision. The orientation and position of the IMUs is shown from a side view in Figure 3-6 and from a front view in Figure 3-7.

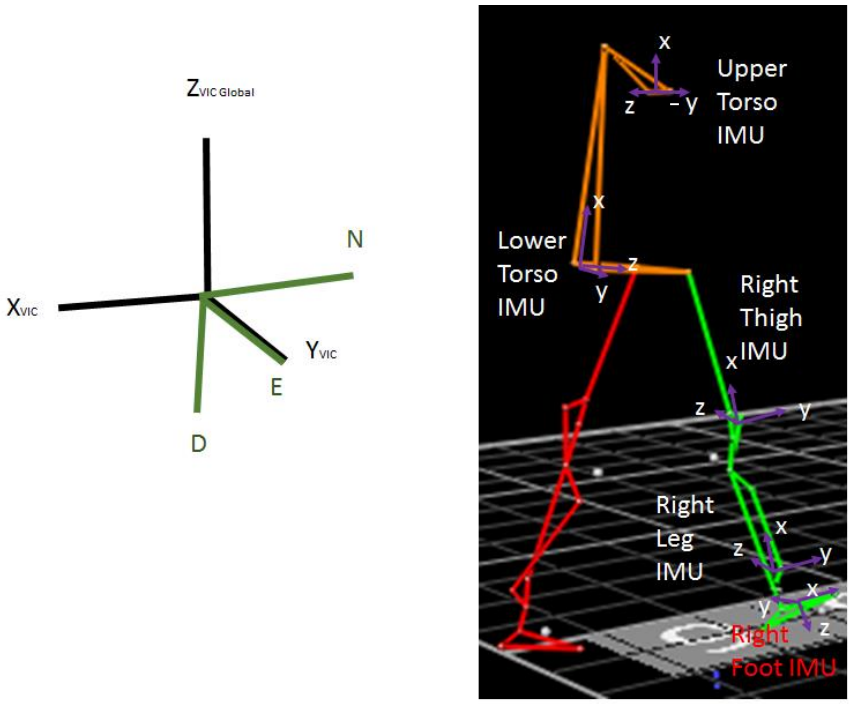

Figure 3-6 Side view of the IMU Body Coordinate Frames

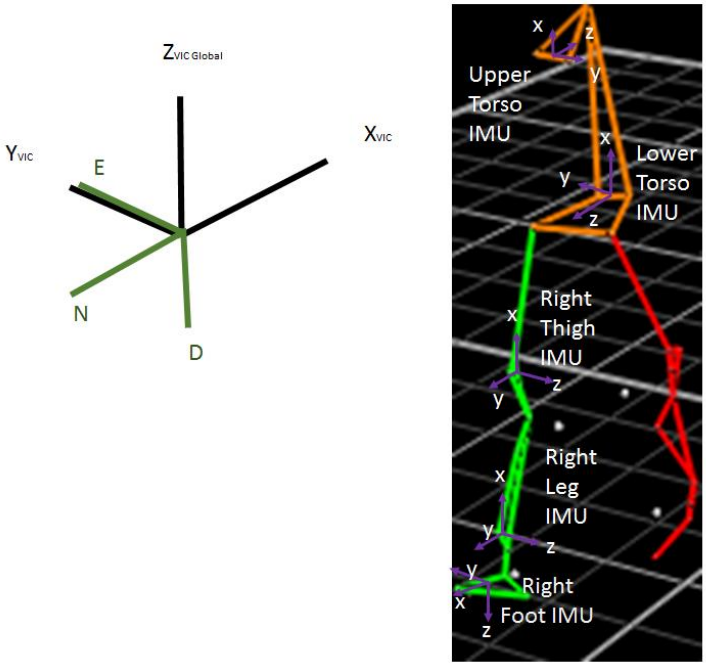

Figure 3-7 Front view of the IMU Body Coordinate Frames

The Vicon® Body Frames are reference frames that track the motion of limbs. Each of these reference frames is centered at a Vicon® Marker with an orientation relative to the Vicon® Global Frame that is computed by the procedure defined in 3.3.3 step 2. The orientation of each of the Vicon® Body Frames

changes with participant movement around the Vicon® Motion capture surface in the same manner the orientation of the IMU Body frames change orientation. This means that for a given limb the relative orientation of the Local Vicon® Body Frame relative to the IMU mounted on the limb is constant, the relative orientation of the Vicon® Body Frame to the IMU frame is computed using the procedure described in section 3.3.5.

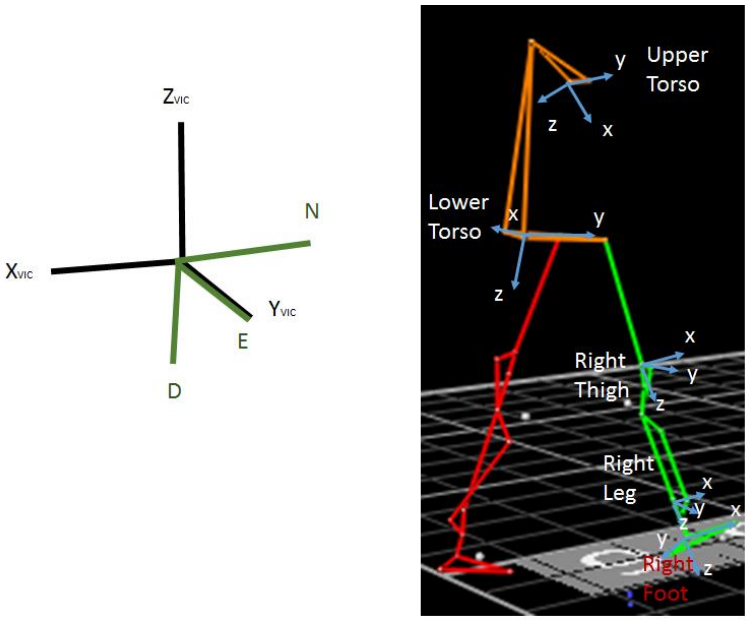

Figure 3-8 Side view of the Vicon Body Coordinate Frames

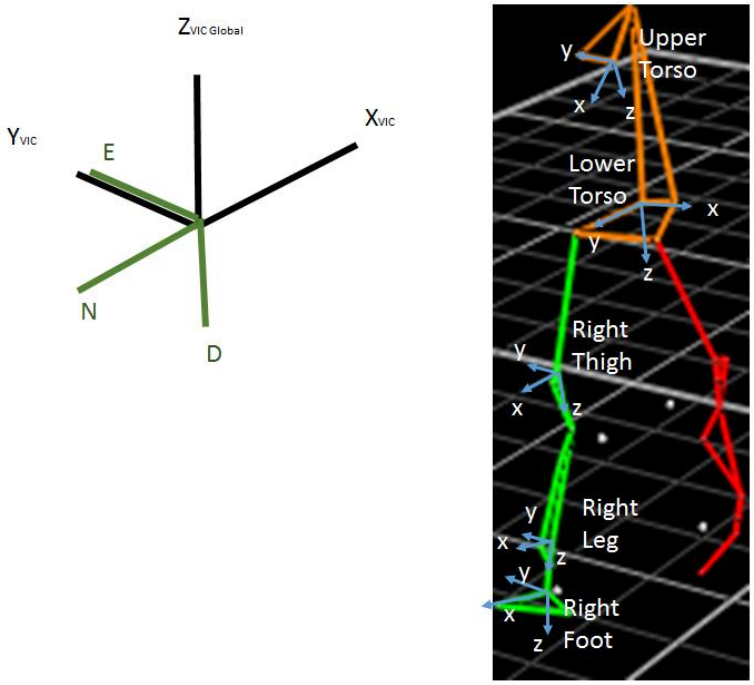

Figure 3-9 Front view of the Vicon Body Coordinate Frames

The table below summarizes the coordinate frames defined to track limb motion.

Coordinate Frame(s)	Number	Location(s)	Orientation
North, East, Down	1	Fixed Point on the lab floor as defined in Vicon® Settings	X – North, Y – East, Z - Down
Vicon Global	1	Fixed Point on the lab floor as defined in Vicon® Settings	Z-Up, Y- Perpendicular to X and Z, X-Opposite the direction of initial travel
IMU Body	5	Fixed to the Upper Torso, Lower Torso, Right Thigh, Right Leg, and Right Foot	X – Out the Connectors of the IMU, Y – Pointed out the right of the IMU, Z – Pointed toward the IMU flat mounting surface
Vicon Local	5	Fixed to the Upper Torso, Lower Torso, Right Thigh, Right Leg, and Right Foot	Varies between each limb depending on the placement of the marker set used to track the limb

In general, navigation output results will be described in the North, East, Down (NED) coordinate system while IMU sensor outputs and Vicon derived inertial data will be described in the local IMU Body coordinate frames for convenience.

3.3 DATA PRE-PROCESSING

The process of transforming raw Vicon and IMU data into quantities that are useful for analyze the turning motion is described in this section. This process is performed for each of the approximately five IMUs for every one of the eight runs for all eight subjects (about 320 different IMU data time histories). Due to the sheer amount of data present it is necessary to process the data efficiently and without human interaction at every step. Figure 3-10 provides an overview of the process used to transform raw IMU data and Vicon data to time and coordinate frame synchronized data capable of providing independent measures of limb kinematic quantities.

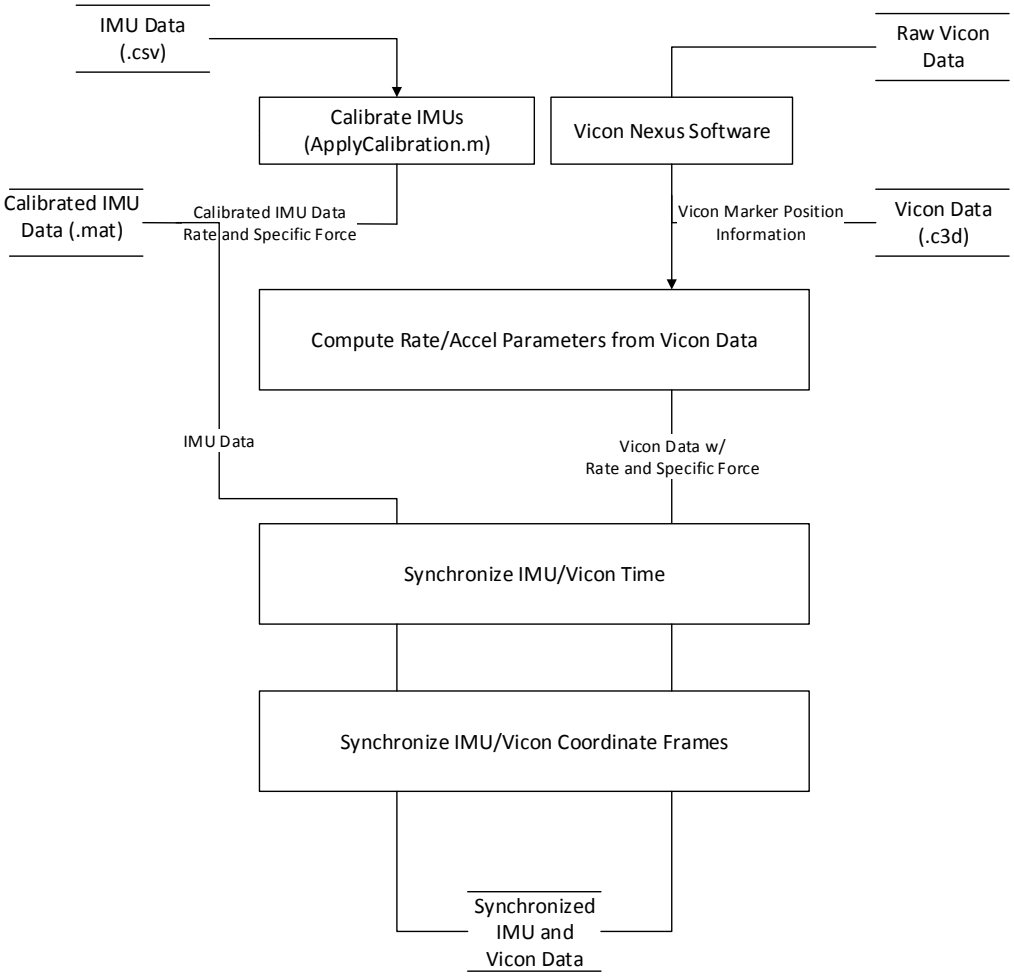

Figure 3-10 The pre-processing of Inertial Measurement Unit (IMU) and Vicon Data

3.3.1 IMU Calibration

IMU calibration removes errors from the Inertial Measurement Unit by comparing output IMU data to specific force and angular rate quantities provided by a rate table. The process produces twenty four quantities per IMU that map the raw voltages output by the 3 gyroscopes and 3 accelerometers in each sensor axes to angular rate and acceleration quantities sensed in the IMU body axis. The mapping between the vector of three A/D converted counts of measured voltages output by the three accelerometers, $\vec{v}^{Accel\_Body}$, and the vector of three specific force quantities in the IMU_Body frame, $\vec{f}^{IMU\_Body}$, is given by equation (3.3.1):

$$\vec{f}^{IMU\_Body} = T_{Accel\_Body}^{IMU\_Body}\vec{v}^{Accel\_Body} + \overrightarrow{\delta f}^{IMU\_Body} \tag{3.3.1}$$

The matrix $T_{Accel\_Body}^{IMU\_Body}$ is a 3x3 transformation that does not necessarily have the properties of a direction cosine matrix and contains accelerometer scale factor, misalignment, and non-orthogonality quantities.

The mapping between the vector of three A/D converted counts of measured voltages output by the three gyroscopes, $\vec{v}^{Gyro\_Body}$, and the vector of three angular rate quantities in the IMU_Body frame, $\vec{\omega}^{IMU\_Body}$, is given by equation (3.3.2):

$$\vec{\omega}^{IMU\_Body} = T_{Gyro\_Body}^{IMU\_Body}\vec{v}^{Gyro\_Body} + \delta\vec{\omega}^{IMU\_Body} \tag{3.3.2}$$

The matrix $T_{Accel\_Body}^{IMU\_Body}$ is a 3x3 transformation that does not necessarily have the properties of a direction cosine matrix and contains gyroscope scale factor, misalignment, and non-orthogonality quantities.

3.3.2 Vicon Nexus Software Processing

The Vicon® Nexus Software allows the user to create data labels associated with position time histories of reflective markers tracked by the infrared camera system in the lab. This is a manual process by which the labels are assigned to each of the markers allow it to be associated with a limb and an IMU. The Vicon Nexus Software is useful to visualize marker location on the subject and observe quality of data and patterns in the gait. This software also interpolates points in time where the camera system was not tracking a reflective marker.

3.3.3 Angular Rate and Specific Force Calculation from Vicon® Data

In order to make a direct comparison between the IMU outputs and the data produced by the Vicon® system it is useful to derive angular rate and specific force quantities from the position time history of three Vicon® markers attached to the same rigid body the IMU is mounted on. This comparison is used to synchronize the IMU/Vicon® time and coordinate frames as described in Sections 3.3.4 and 3.3.5 and to identify any issues with the IMU measurement data.

The Vicon derived angular rate and specific force data can also be used to test the Strapdown Navigation algorithms described by the process in section 3.3.4 .

The angular rate and specific force calculation takes place in four steps as shown in *Figure 3-11*:

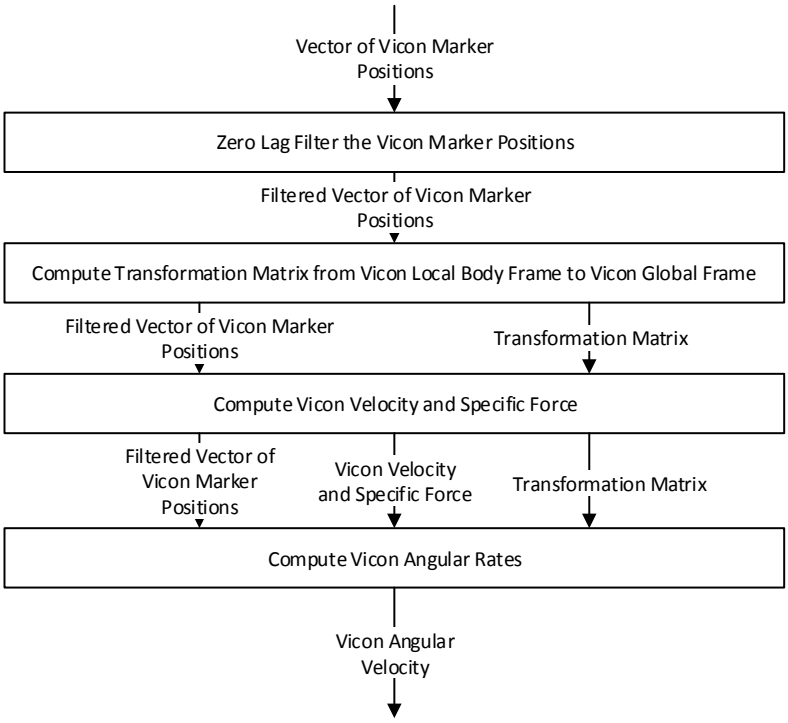

Figure 3-11 Process of computing specific force and angular rate from the three Vicon position vectors for each limb

Details of these steps are as follows

1. Low pass filter the position time history vector output from the Vicon Nexus Software

   The output of the Vicon® Nexus Software is a 120 Hz frequency time history of the marker position expressed in the Vicon® Global Frame denoted $\vec{r}_i^{\,V}$ with *i* being an integer indicating the marker number. Since this data is sampled at a high rate it contains frequency contents at higher frequencies which may be amplified by the numerical differentiation process. To prevent the amplification of

these high frequency components the position vector of each Vicon marker is put through a zero phase low pass Butterworth Filter with a cut-off frequency of 8 Hz. The filter is defined using the Matlab *butter()* command and the zero phase filtering is performed using the Matlab *filtfilt()* command.

2. Form the Vicon® Body Frame to Vicon® Global Frame direction cosine matrix for each Vicon® epoch from the set of markers attached to the rigid limb

   The output of the Vicon® Nexus Software is a time history of the marker position expressed in the Vicon® Global Frame denoted $\vec{r}_i^{\,V}$ with *i* being an integer indicating the marker number. Each joint has three markers with indices, *i*, numbered from 1-3 that are used to define a local Vicon® Body Frame as shown in Figure 3-12.

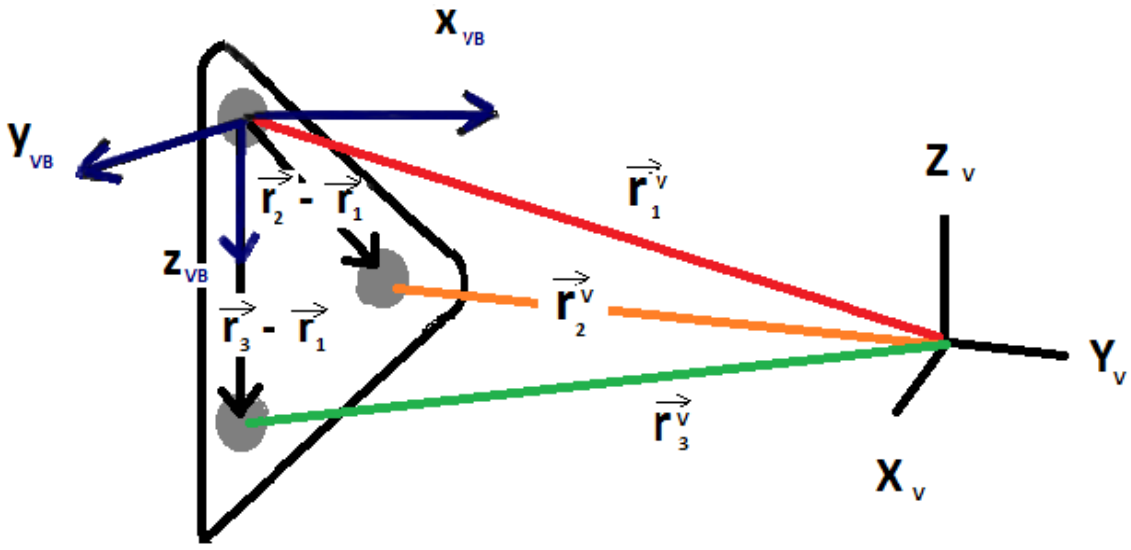

Figure 3-12 The quantities used to form the Vicon Body Frame

In order to define a frame that is fixed relative to the orientation of the marker placard shown in Figure 3-12, take the difference of the Vicon® marker positions:

$$\vec{r}_{12}^{\,V} = \vec{r}_2^{\,V} - \vec{r}_1^{\,V} \tag{3.3.3}$$

$$\vec{r}_{13}^{\,V} = \vec{r}_3^{\,V} - \vec{r}_1^{\,V} \tag{3.3.4}$$

This gives two vector quantities that point along the lines between the markers which are fixed in direction when viewed from the frame of marker 1. These vector quantities are used to define the axes of the Vicon® Body Frame. Since the IMU is mounted to the IMU with its X axes approximately aligned along $\vec{r}_{13}^{\,V}$, the direction of $\vec{r}_{13}^{\,V}$ is defined to be the unit vector of the Vicon® Body Frame Z axis.

$$\hat{Z}_{VB}^{V} := \frac{\vec{r}_{13}^{V}}{\left|\vec{r}_{13}^{V}\right|} \tag{3.3.5}$$

To define another line fixed relative to the frame of marker 1 with unit magnitude take the cross product of these two lines and divide it by the magnitude:

$$\hat{Y}_{VB}^{V} := \frac{\vec{r}_{13}^{V} \times \vec{r}_{12}^{V}}{\left|\vec{r}_{13}^{V} \times \vec{r}_{12}^{V}\right|} \tag{3.3.6}$$

The final unit vector of the Vicon® Body Frame is then formed by taking the cross product of the other axes unit vectors:

$$\hat{X}_{VB}^{V} := \hat{Y}_{VB} \times \hat{Z}_{VB} \tag{3.3.7}$$

These three orthogonal unit vectors provide information about the orientation of the Vicon® Body Frame relative to the Vicon® Global Frame. The orientation information can be expressed as a direction cosine matrix through equation (3.3.8) [5]

$$C_{VB}^{V} = \begin{bmatrix} \hat{X}_{VB,x}^{V} & \hat{Y}_{VB,x}^{V} & \hat{Z}_{VB,x}^{V} \\ \hat{X}_{VB,y}^{V} & \hat{Y}_{VB,y}^{V} & \hat{Z}_{VB,y}^{V} \\ \hat{X}_{VB,z}^{V} & \hat{Y}_{VB,z}^{V} & \hat{Z}_{VB,z}^{V} \end{bmatrix} \tag{3.3.8}$$

For each Vicon® epoch this transformation matrix gives information on how the marker set mounted to each limb is oriented relative to the Vicon® global frame. This information is required to form the Vicon® derived specific force and angular rate measurements described in steps 3-4 and to use as a comparison to the navigation solution formed by integrating the IMU data.

3. Compute the velocity and specific force from the Vicon®

Prior to numerical differentiation the position vectors, $\vec{r}_{i}^{V}$, of each marker are zero phase low-pass filtered to avoid amplification of high frequency noise that may occur due to numerical differentiation. For each axis of the marker's position a third order piecewise polynomial is computed with the Matlab command *spline*. This piecewise polynomial is then differentiated twice and each derivative is evaluated at a rate equal to or greater (600 Hz was chosen to evaluate the Strapdown Navigation algorithms described in

section 4) than the original position vector rate (120 Hz). The differentiation and evaluation are computed with the Matlab command *fntlr* which results in the velocity vector of the marker point in the Vicon® Global Coordinate Frame, $\vec{v}_i^V$, and the acceleration vector of the marker point in the Vicon® Global Coordinate Frame, $\vec{a}_i^V$.

The specific force in the Vicon® Global Coordinate Frame for the i^{th} marker, $\vec{f}_i^V$. , is computed by adding the gravity that has been rotated from the NED Frame to the Vicon® Global Coordinate Frame using the transformation matrix defined in .

$$\vec{f}_i^V = \vec{a}_i^V + C_{NED}^V \vec{g}^{NED} \tag{3.3.9}$$

The specific force in the Vicon® Body Frame, $\vec{f}_i^{VB}$, is then computed using the transpose of the attitude DCM determined in step 2 interpolated to the time of validity of the 600 Hz data

$$\vec{f}_i^{VB} = C_V^{VB}\big|_{600\,Hz}\ \vec{f}_i^V \tag{3.3.10}$$

The quantity, $\vec{f}_i^{VB}$, is averaged over all markers to compute the average acceleration then passed to the function used to synchronize the Vicon® and IMU times of validity as described in section 3.3.4.

4. Determine the angular derivative quantities of the Vicon® Body Frame

For each element of the direction cosine matrix computed in step 2 a third order piecewise polynomial is computed with the Matlab command spline. This piecewise polynomial is then differentiated once with the derivative evaluated at a rate equal to or greater than the original position vector rate (120 Hz). 600 Hz was chosen to evaluate the Strapdown Navigation algorithms described in section 4 in order to reduce the algorithmic error from the Euler integration. The differentiation and evaluation are computed with the Matlab command *fntlr* which results in the time derivative of the direction cosine matrix which describes the rotation from the Vicon® Body Frame to the Vicon® Global Frame, $\dot{C}_{VB}^V$. The angular rate is then computed as follows:

$$\Omega_{V/VB}^{VB} = C_V^{VB}\dot{C}_{VB}^V \tag{3.3.11}$$

The quantity $\vec{\omega}_{V/VB}^{VB}$ is taken from the skew symmetric elements of $\Omega_{V/VB}^{VB}$ and then passed to the function used to synchronize the Vicon® and IMU times of validity as described in section 3.3.4

3.3.4 Vicon/IMU Time Synchronization

The particular IMUs used in this experiment have angular rate and specific force measurements that are not necessarily output at a constant rate. To allow for a single time offset to be computed for the both the angular rate and specific force data set each of these quantities is interpolated to the same integer multiple time which is defined by equation (3.3.12):

$$t_{IMU} = [1, 2, 3, \ldots N] * \left(\frac{1}{100} \right) \tag{3.3.12}$$

The interpolation is then performed for both the angular rate and specific force using the Matlab function *interp1*

$$\vec{f}^{\,IMU\_b}\,|_{t_{IMU}} = interp1\left(t_{f,} \vec{f}^{\,IMU_b}\,|_{t_f}, t_{IMU} \right) \tag{3.3.13}$$

$$\vec{\omega}_{IMU_b/I}^{IMU\_b}\,|_{t_{IMU}} = interp1\left(t_{f,} \vec{\omega}_{IMU_b/I}^{IMU\_b}\,|_{t_f}, t_{IMU} \right) \tag{3.3.14}$$

The specific force and angular rate data generated from the Vicon® position measurements and measured from the IMU are not valid at the same time of validity and are not expressed in the same coordinate frame, but contain similar underlying dynamics since they are both are derived from measurements of motion of the same limb. Even though the vectors are valid in different coordinate frames the magnitude of the vector is coordinate frame invariant. This means that the norm of the vector is preserved in the transformation between the IMU body coordinate frame and Vicon® Body coordinate frame. This means that the norm of the vector is independent what frame it is expressed in which makes it usefully for observing the time offset of the IMU and Vicon® Body Frame quantities. The norm of a vector is defined as

$$\left| \vec{v} \right| = \sqrt{v_x^{\,2} + v_y^{\,2} + v_z^{\,2}} \tag{3.3.15}$$

To eliminate coordinate frame dependence of the dynamics, the norm of the Vicon® specific force, $\vec{f}_i^{\,VB}$, Vicon® angular rate, $\vec{\omega}_{VB/V}^{VB}$, IMU specific force, $\vec{f}_i^{\,IMU\_b}\,|_{t_{IMU}}$, and IMU angular rate, $\vec{\omega}_{IMU_b/I}^{IMU\_b}\,|_{t_{IMU}}$, are taken. Aside from measurement errors the difference between the norms of the Vicon® derived inertial measurements and the inertial measurements from the IMU is the time offset between them. In order to measure the time offset between the specific force quantities the cross correlation between the norm of the IMU specific force and norm of the Vicon® specific force is computed using the Matlab *xcorr* command:

$$\left[f_{corr}, l_{f_{corr}} \right] = xcorr\left(\left| \vec{f}_i^{IMU\_b} \right|_{t_{IMU}} \right|, \left| \vec{f}_i^{VB} \right| \right) \tag{3.3.16}$$

Similarly, the cross correlation between the norm of the IMU angular rate and norm of the Vicon® angular rate is computed

$$\left[\omega_{corr}, l_{\omega_{corr}} \right] = xcorr\left(\left| \vec{\omega}_{IMU_b/I}^{IMU\_b} \right|_{t_{IMU}} \right|, \left| \vec{\omega}_{VB/V}^{VB} \right| \| \| \right) \tag{3.3.17}$$

The cross correlation is a measure of the similarity of each of the vectors, captured by the first output from *xcorr*, when one is shifted in index relative to the other. In the case of these time measured quantities, the index difference equates to a time offset between the IMU and the Vicon® measurement times. The lag offset used to compute the correlation value between the input vector quantities is the second output from *xcorr* represented in equations (3.3.16) and (3.3.17) as *l*.

The lag offset given by equation (3.3.17) is used to determine the time offset between the Vicon® angular rate and IMU angular rate. The lag offset at the index of the maximum correlation (max(ω_{corr})) between Vicon® and IMU angular rate measurements corresponds to an IMU time when lag > 0 and Vicon® time when lag < 0. The offset between the angular rate time of the Vicon and the angular rate time of the IMU is then given by:

$$\delta t_{\omega,IMU/VIC} = \begin{cases} t_{IMU}\left(l_{\omega_{corr}}\left(i_{\omega_{corr,max}}\right) + 1\right) - t_V(1), lag > 0 \\ t_{IMU}(1) - t_V\left(l_{\omega_{corr}}\left(i_{\omega_{corr,max}}\right) + 1\right), lag < 0 \end{cases}$$

The lag offset given by equation (3.3.16) is used to determine the time offset between the Vicon specific force and IMU specific force. The lag offset at the index of the maximum correlation (max(f_{corr})) between Vicon® and IMU specific force measurements corresponds to an IMU time when lag > 0 and Vicon® time when lag < 0. The offset between the specific force time of the Vicon and the specific force time of the IMU is then given by:

$$\delta t_{f,IMU/VIC} = \begin{cases} t_{IMU}\left(l_{f_{corr}}\left(i_{f_{corr,max}}\right) + 1\right) - t_V(1), lag > 0 \\ t_{IMU}(1) - t_V\left(l_{f_{corr}}\left(i_{f_{corr,max}}\right) + 1\right), lag < 0 \end{cases}$$

The Vicon® time of angular rate and specific force represented in the same time base as the IMU time can then be written as:

$$t_{\omega,V@IMUt} = t_{\omega,V} + \delta t_{\omega,IMU/VIC} \tag{3.3.18}$$

$$t_{f,V@IMUt} = t_{f,V} + \delta t_{f,IMU/VIC} \tag{3.3.19}$$

Since the angular rate and specific force data from the IMU were interpolated to the same times of validity these quantities should have the same value. If these quantities are not similar to within 1 100 Hz (0.01 s) frame a warning is written for the user to notify them of inconsistencies in time base alignment between the angular and linear derivative quantities. If the quantities are similar within 1 100 Hz (0.01 s) the Vicon® time used for comparison to the IMU is arbitrarily chosen to be the Vicon® specific force time. Since the specific force and angular rate quantities are largely independent of one another this serves as a check of the consistency of the IMU and Vicon Data. Consider a case where the IMU and the Vicon data are completely inconsistent with one another. In this case it is unlikely that the inconsistency of the Vicon angular rate and IMU angular rate is nearly exactly the same as the inconsistency of the Vicon specific force and IMU specific force. When the inconsistencies are different the cross correlations give distinct offset values leading to different time offset values leading the data to fail the 1 100 Hz sample consistency check.

3.3.5 Vicon/IMU Coordinate Frame Transformation Determination

After time synchronization the Vicon® and IMU angular rates and specific force measurements are valid at approximately the same times but are represented in different body axis coordinate frames. In order to compare kinematic and navigation quantities for each limb between the IMU and the Vicon® it is necessary to compute the transformations between their frames of reference. Since the IMU and the Vicon® sensors are attached to the same rigid body they are measuring the same specific force and the relative orientation of the Vicon® Body Frame and the IMU Body Frame are not changing (Section 3.2). For a single time-aligned measurement from both systems assume there is a transformation matrix that maps the specific force in the IMU Body Frame to the Vicon® Body such that equation (3.3.20) holds.

$$\vec{f}^{\,V} = C^{VB}_{IMU_b}\,\vec{f}^{\,IMU_b} \tag{3.3.20}$$

Since the quantity $C^{V}_{IMU_b}$ is not changing this equation holds for the entire set of data containing N elements where both IMU and Vicon® specific force measurements are available.

$$\vec{f}^{VB}(1) = C_{IMU_b}^{VB}\vec{f}^{IMU}(1)$$

$$\vec{f}^{V}(2) = C_{IMU_b}^{VB}\vec{f}^{IMU}(2) \tag{3.3.21}$$

$$\vdots$$

$$\vec{f}^{V}(N) = C_{IMU_b}^{VB}\vec{f}^{IMU_b}(N)$$

This is now a matrix algebra problem where the solution is the 3x3 matrix, C_{IMU}^{V}, and the inputs are two 3xN matrices defined to be *X* and *x*:

$$X = \left[\vec{f}^{VB}(1), \vec{f}^{VB}(2), \cdots, \overrightarrow{f}^{VB}(1)\right]^{\mathrm{T}} \tag{3.3.22}$$

$$x = \left[\vec{f}^{IMU\_b}(1), \vec{f}^{IMU\_b}(2), \cdots, \overrightarrow{f}^{IMU\_b}(1)\right]^{\mathrm{T}} \tag{3.3.23}$$

The least squares solution to the problem is then given by equation(3.3.24):

$$C_{IMU_b,ls}^{VB} = Xx^{\mathrm{T}}\left(xx^{\mathrm{T}}\right)^{-1} \tag{3.3.24}$$

This is the theoretical solution to the problem, however in practice the data contains errors due to imperfect ability of the IMU and the Vicon™ to measure the specific force. These errors cause the nominally unitary transformation matrix to be non-unitary so to obtain the final form of the transformation matrix constrain the transformation matrix to a unitary, symmetric matrix using the singular value decomposition (Mathworks).

$$[U_C, \omega_{C,diag}, V_C] = svd\left(C_{IMU_b,ls}^{V}\right) \tag{3.3.25}$$

The transformation matrix can then be computed using the upper triangular and lower triangular outputs from the singular value decomposition algorithm.

$$C_{IMU_b}^{V} = U_C V_C^{\mathrm{T}} \tag{3.3.26}$$

This transformation matrix is used to initialize IMU Navigation from the Vicon heading and compare kinematic quantities between the Vicon and the IMU.

4 Navigation Algorithms

This section describes the algorithms used in navigation of the foot mounted IMU and the attitude estimation of the trunk mounted IMU.

4.1 NAVIGATION OF THE FOOT USING ZUPTS

This section describes the equations used to implement the inertial navigation solution on the foot mounted sub-system with zero velocity pseudo-measurements (ZUPTs) during foot stance phase processed by an Extended Kalman Filter (EKF). The inertial navigation and EKF code is implemented in Matlab and acts on recorded IMU data in a causal manner, the code is adapted from INS/GPS sensor fusion code (Gebre-Egziabher).

The quantities of interest for a navigation system are the position in the North, East, Down (NED) coordinate frame, $\vec{p}_{ins}^{NED}$, the velocity in the NED coordinate frame, $\vec{v}_{ins}^{NED}$, and the Euler angles which describe the rotation between the sensor body frame and the NED frame, $\vec{\gamma}_{ins}$. The sub-script *ins* refers to the fact that the quantities are produced by an inertial navigation system; this system makes use of an IMU in the initialization and propagation of the navigation solution. As described in Section 3.1.2 the IMU contains a number of error sources that significantly degrade navigation performance.

The EKF estimates the errors in the navigation states as well as the incremental error in the current computed bias value for each of the three accelerometers, $\delta\vec{b}_f$, and each of the three gyroscopes, $\delta\vec{b}_\omega$.

$$\vec{x} = [\delta\vec{p}_{ins}^{NED}, \delta\vec{v}_{ins}^{NED}, \delta\vec{\gamma}_{ins}, \delta\vec{b}_f, \delta\vec{b}_\omega\ ]^{\mathrm{T}} \tag{4.1.1}$$

The remainder of the IMU errors are assumed to be negligible.

4.1.1 Filter and Navigation Initialization:

The initialization of the system can be separated into navigation solution initialization and EKF state and uncertainty initialization. Since GNSS satellites are not available in the lab environment the navigation solution computed in this experiment is initialized by slightly different means than the integrated GNSS/INS pedestrian navigation solutions described in section 1.2. The initial position of the limb being tracked in Latitude, Longitude and Altitude is given as the sum of the known Latitude, Longitude and Altitude of the Vicon Global Coordinate frame and relative position of the limb the navigation system is attached to, scaled into radians for Latitude and Longitude and meters for altitude.

The initial uncertainty in the position error state set in the EKF is set to be 5 meters, since that is accuracy of the position the origin of the Vicon coordinate system is known to and the accuracy of the vector from

the Vicon Global Coordinate Frame origin is known to much greater precision. The initial velocity of the system is set to zero in all axes since the participant is still at the beginning of the experiment.

The initialization of tilt attitude makes use of the assumption that the person is stationary during the alignment period described in Section 3.1 and completely still and the specific force sensed by the accelerometers is only due to gravity. This still period is detected by examining the first 10 seconds of the trajectory for a periods of time where the magnitude of the specific force minus gravity is less than 3 times the expected accelerometer bias.

$$t_{still} := \sqrt{f_{ib,x}^2 + f_{ib,y}^2 + f_{ib,z}^2} - g < 3\sigma_{\delta b_f} \tag{4.1.2}$$

The initial pitch and roll angles can then be computed from the average specific force over the still period by trigonometry with respect to the gravity vector which points mostly in the down direction.

The initial heading angle is then determined from the Vicon attitude using the transformation between the Vicon Global and NED frames as the average initial transformation between Vicon Local Frame and NED frame during the still period, as computed in Section 3.3.3 Step 2, and the transformation between the Vicon Local Frame and the IMU frame as computed in Section 3.3.5.

$$C_{IMU_b}^{NED} = C_V^{NED} \overline{C_{VB}^V} C_{IMU_b}^{VB} \tag{4.1.3}$$

The heading angle can be computed from Equation (4.1.4):

$$\psi_0^{Foot} = atan2\left(C_{IMU_b}^{NED}(1,2), C_{IMU_b}^{NED}(1,1)\right) \tag{4.1.4}$$

During the still period the gyro bias can also be computed as the average angular rate measured by the gyroscopes.

$$\vec{b}_\omega = \overline{\vec{\omega}}_{IMU_b/I}^{IMU_b} \tag{4.1.5}$$

This value is then used as the initial value of the gyro bias used to compute the attitude of the limb by the inertial navigation system. The initial accelerometer bias values are set to zero since they cannot be observed during the stationary period. The initial state values of the EKF are set to zero since the initial navigation quantities incorporate all known information about the state of the system prior to motion.

$$\vec{x}_0 = \left[0_{15X1}\right] \tag{4.1.6}$$

The initial uncertainty of the navigation states is used to initialize the covariance of the EKF. The initial navigation state errors are assumed to be uncorrelated with the other states making the P_0 matrix diagonal.

4.1.2 INS Update and Kalman Filter Time Update:

During periods of time where the EKF has no measurements the navigation state of the limb is computed by integrating the measured specific force and angular rate and the uncertainties of the EKF state estimates are propagated forward in time according to the state transition matrix and the process noise.

For simplicity, the navigation state computation is performed in the local level frame assuming the sensors used are automotive grade with and many of the terms that contribute to the errors in navigation are negligible compared to the sensor quality. The simplified equations are implemented as described in Chapter 6 of (Gleason and Gebre-Egziabher)

Angular rate is integrated into attitude using equation (4.1.7):

$$\begin{bmatrix} \phi_k^{Foot} \\ \theta_k^{Foot} \\ \psi_k^{Foot} \end{bmatrix} = \begin{bmatrix} \phi_{k-1}^{Foot} \\ \theta_{k-1}^{Foot} \\ \psi_{k-1}^{Foot} \end{bmatrix} + F_{Tr}^{Euler} \vec{\omega}_{\text{Foot}/NED,k-1}^{Foot} (t_k - t_{k-1}) \tag{4.1.7}$$

With the transformation between body rate and Euler rate as shown in equation (4.3.2).

$$F_{Foot}^{Euler} = \begin{bmatrix} 1 & \sin\phi_{k-1}^{Foot} \tan\phi_{k-1}^{Foot} & \cos\phi_{k-1}^{Foot} \tan\theta_{k-1}^{Foot} \\ 0 & \cos\phi_{k-1}^{Foot} & -\sin\phi_{k-1}^{Foot} \\ 0 & \dfrac{\sin\phi_{k-1}^{Foot}}{\cos\theta_{k-1}^{Foot}} & \dfrac{\cos\phi_{k-1}^{Foot}}{\cos\theta_{k-1}^{Foot}} \end{bmatrix} \tag{4.1.8}$$

The specific force measured by the accelerometer is then rotated into the navigation frame:

$$f_{Foot/I,k}^{NED} = C_{IMU_b,k}^{NED} f_{Foot/I,k}^{IMU_b} \tag{4.1.9}$$

Where $C_{IMU_b}^{NED}$ is computed using the Euler angles computed using the Euler Angle to Direction Cosine Matrix Routine described in Section 8.2 with the input Euler Angles being the values computed by equation (4.1.7). Given that the application is personal navigation the Coriolis force can be neglected reducing the velocity update equation to Equation (4.1.10).

$$\mathrm{v}_k = \mathrm{v}_{k-1} + (f_{Foot/I,k}^{NED} - g^{NED})(t_k - t_{k-1}) \tag{4.1.10}$$

At each time update step the Kalman Filter covariance is propagated forward in time using equation (4.1.11). The definition and structure of can be found in [8], chapter 6 equations 6.21-6.23, and the detail of derivation can be found in [9] pg. 384 – 388.

$$P_k^- = \Phi_{k-1} P_{k-1}^+ \Phi_{k-1}^T + Q_{k-1} \tag{4.1.11}$$

If a measurement is not available the values of the state and covariance on the next time step are set to the *apriori* values, otherwise if a measurement is available the measurement update is performed as described in Section 4.1.3.

4.1.3 Measurement Update

In the pedestrian navigation application filter that makes use of Zero Velocity Updates (ZUPTs) that are asynchronous in nature since the measurement update takes place whenever the zero velocity condition is declared. For this experiment the zero velocity condition is declared when the Vicon™ System determines that the foot mounted marker has a filtered velocity, as computed in Section 3.3.3, that is less than 0.05 m/s, and it has been greater than 0.1 seconds since the last ZUPT measurement was declared valid. This second condition is critical to prevent the filter from becoming unstable due to a collapsed covariance resulting from the processing of a large number of measurements in a short period of time. For each measurement update the Kalman gain is computed using equation (4.1.12).

$$L_k = P_k^- H^T (H P_k^- H^T + R_k)^{-1} \tag{4.1.12}$$

Where P_k^- is the covariance computed during the Kalman Filter time update, H is as computed using equation (4.1.13), and R_k is defined using equation (4.1.14). This definition of R_k prevents the filter from too heavily weighting the measurement and causing the covariance to collapse, and instead gradually remove the error over the course of the foot stance phase [6].

$$H = \begin{bmatrix} 0_{3X3} & I_{3X3} & 0_{3X3} & 0_{3X6} \end{bmatrix} \tag{4.1.13}$$

$$R_k = I_{3x3} \times \max(trace(H P_k^- H^T)) \tag{4.1.14}$$

The innovation is then formed using equation (4.1.15)with the y vector being 0_{3x1}, H being given in equation (4.1.13), and $\vec{x}_k^-$ being computed by the time update process. Making these substitutions the z vector is just the velocity at the time when the zero velocity condition is detected.

$$\vec{z} = \vec{y} + H\vec{x}_k^- \tag{4.1.15}$$

The updated state is the weighted difference between the *apriori* state, $\vec{x}_k^-$, and the feedback given by $L\vec{z}$ as shown in equation (4.1.16).

$$x_k^+ = \vec{x}_k^- - L\vec{z} \tag{4.1.16}$$

The *aposteriori* state uncertainty is then computed using equations (4.1.17) and (4.1.18).

$$P_k^+ = \frac{1}{2}\left(I_{15x15} - L_k H\right) P_k^- \tag{4.1.17}$$

$$P_k^+ = \frac{1}{2}\left(P_k^+ + (P_k^+)^{\mathrm{T}}\right) \tag{4.1.18}$$

By performing the covariance updated the filter is initialized for the next time-update step. More detail on the application of Kalman Filters to foot mounted personal navigation devices can be found in [6] and [9], more detail on Kalman Filtering can be found in [20].

4.2 TURNING DETECTION ALGORITHM

Accurate identification of straight line motion segments is key for the trunk attitude determination sub-system operation. If the onset of turning is not detected on the stride in which the turn occurs, the information about the trunk rotation is discarded. That is, the trunk attitude, Ψ_{s-1}^{Tr}, used in equation (4.3.4) is only stored for one stride as shown in Figure **2-4** in order to minimize the contribution of gyro drift error that integrated into Ψ_s^{Tr}. If the turning segment end is declared prematurely, the attitude update will introduce error. This is because the assumption that attitude is constant is not valid. The error in the attitude will be present is equal to the amount of angular motion not removed by the trunk attitude filter gain. If, however, the turning segment end is declared late, error due to uncorrected gyro drift will accumulate.

The thresholds for detection of turning motion presented here have been experimentally determined. They are given in **Table 2** and are consistent with an IMU using gyros with the error model parameters given in **Table 1**. If a different IMU is used, the thresholds should be changed to be consistent with the error characteristics of the IMU/gyros used.

Figure 4-1 is a high-level depiction of the turn detection sub-system. The input to the detection logic are the estimates of $\Delta\psi_T$, $\Delta\phi_T$, $\Delta\psi_F$ and SW. The first two of these are calculated by the trunk attitude sub-system as shown in **Figure 9**. The remaining two are calculated from the outputs of the foot-mounted sub-system. **Figure 4-2** shows how they are calculated.

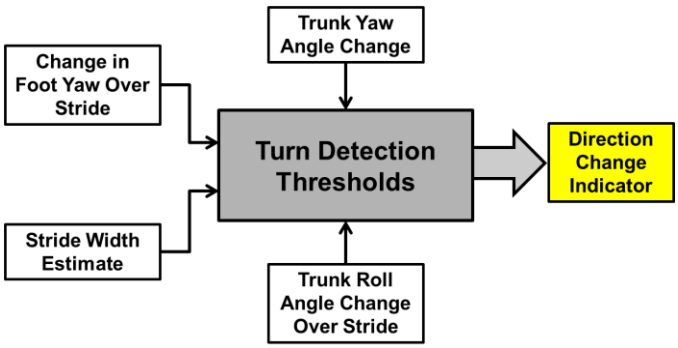

Figure 4-1 High Level View of the Turn Detection Algorithm

Using the right foot as shown in Figure 5 as an example, the change in foot yaw over a stride between the $(k+1)^{th}$ and the k^{th} step, $\Delta\psi_{F,k+1}$ can be computed from the foot-mounted sub-system using the following equation:

$$\Delta\psi_{F,k+1} = \psi_{F,k+1} - \psi_{F,k} \tag{4.2.1}$$

Similarly, the stride width SW is determined by noting that it is equal to the perpendicular distance (relative to a line in the direction of motion) the foot travels from ground-contact to ground-contact. It can be computed using the position vector estimates, $\mathbf{p}^{NED}$, made by the EKF in the foot-mounted system using the following equation:

$$SW = \left\| \left(\mathbf{p}_{k+1}^{NED} - \mathbf{p}_{k}^{NED} \right) - \left(\left\| \mathbf{p}_{k+1}^{NED} - \mathbf{p}_{k}^{NED} \right\| \right) \bullet \hat{\mathbf{u}} \right\| \tag{4.2.2}$$

where is the unit vector $\hat{\mathbf{u}}$ is parallel to the line connecting the foots position at time step *k* and *k-1*. Mathematically, this is given by:

$$\hat{\mathbf{u}} = \frac{\mathbf{p}_{k}^{NED} - \mathbf{p}_{k-1}^{NED}}{\left\| \mathbf{p}_{k}^{NED} - \mathbf{p}_{k-1}^{NED} \right\|} \tag{4.2.3}$$

The stride width can be thought of as the magnitude of the observed change in NED direction made over the stride minus the predicted change in NED direction if the person were to continue walking in a straight line.

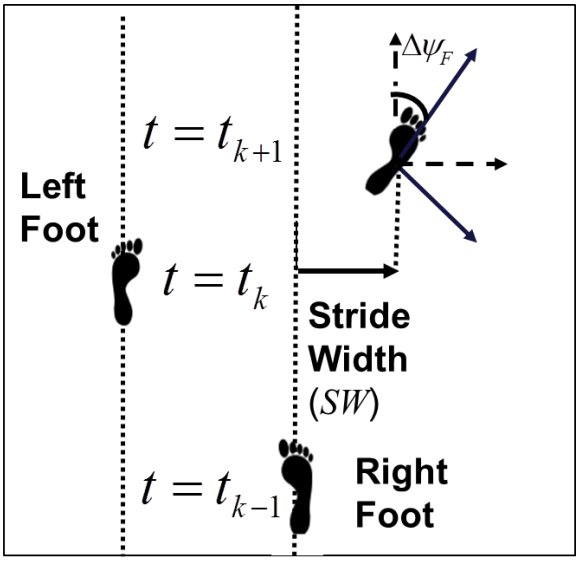

Figure 4-2 Illustration of a turning stride

The input turning detection parameters from the torso can be computed with the aid of Figure 4-3 and Figure 4-4. The change in trunk roll over a stride is computed from the output of the trunk mounted x-gyroscope as shown in Equation (4.2.4).

$$\Delta\phi^{Tr} = \phi^{Tr}_{RFC,k+1} - \phi^{Tr}_{RFC,k} \tag{4.2.4}$$

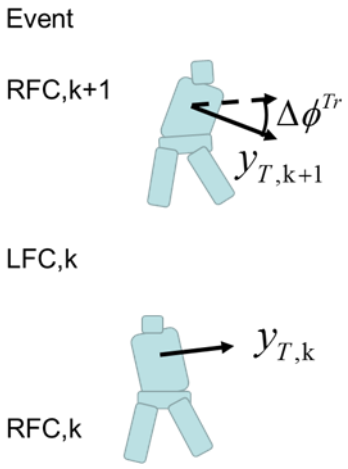

Figure 4-3 The definition of the change in trunk roll parameter

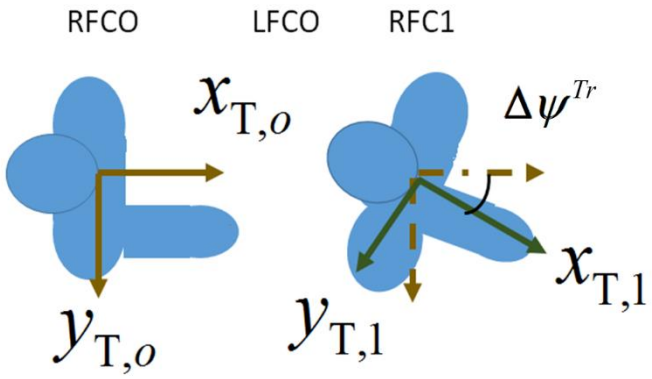

Figure 4-4 Illustration of the change in trunk heading

The change in trunk yaw over a stride is computed from the output of the trunk mounted z-gyroscope as shown in equation (4.2.5).

$$\Delta\psi^{Tr} = \psi^{Tr}_{RFC,k+1} - \psi^{Tr}_{RFC,k} \qquad (4.2.5)$$

After the computation of these parameters over a stride segment the absolute value of each parameter is compared to a threshold. If two out of four parameter values shown in **Figure 4-1** are greater than their specified threshold shown in **Table 2**, motion is considered to be straight line motion, otherwise a stride is considered to be turning motion. These thresholds are determined experimentally from data for the eight subjects and is shown.

Table 2 The turning threshold parameters

Turning Parameter	Threshold
Stride Width (SW)	15 cm
$\Delta\psi_{RF}$	5 (deg)
$\Delta\phi_{Tr}$	3 (deg)
$\Delta\psi_{Tr}$	3.5 (deg)

By eliminating strides that have out of characteristic parameters that show the effects of turning the possibility of filtering out real motion through the attitude update filter is reduced. The attitude threshold parameters function like a measurement rejection test in a Kalman Filter for the attitude filter even if no other parameters indicate a turn. That is if the individual attitude parameter is larger than its threshold that measurement is not processed.

4.3 NAVIGATION INCORPORATION OF TURNING DETECTION ALGORITHM

To form the attitude measurement for the current right foot contact, which is effectively used to constrain the motion of the trunk to a straight line path, the initial attitude must be known. The initial attitude of the trunk is assumed to be known before the user enters a GNSS-denied area. At the start, this attitude is used to initialize the trunk sub-system.

After initialization of the trunk attitude, the next step is to integrate the trunk mounted three axis gyroscope outputs to compute the change in trunk attitude over the period between the stride start and stride end. For each IMU sample, *k*, with $t_{s-1} \le t_k < t_s$ the attitude is updated from the IMU output using equation (4.3.1)

$$\begin{bmatrix} \phi_k^{Tr} \\ \theta_k^{Tr} \\ \psi_k^{Tr} \end{bmatrix} = \begin{bmatrix} \phi_{k-1}^{Tr} \\ \theta_{k-1}^{Tr} \\ \psi_{k-1}^{Tr} \end{bmatrix} + F_{Tr}^{Euler} \vec{\omega}_{Tr/NED,k-1}^{Tr} (t_k - t_{k-1}) \tag{4.3.1}$$

With the transformation between body rate and Euler rate as shown in equation (4.3.2).

$$F_{Tr}^{Euler} = \begin{bmatrix} 1 & \sin\phi_{k-1}^{Tr} \tan\phi_{k-1}^{Tr} & \cos\phi_{k-1}^{Tr} \tan\theta_{k-1}^{Tr} \\ 0 & \cos\phi_{k-1}^{Tr} & -\sin\phi_{k-1}^{Tr} \\ 0 & \dfrac{\sin\phi_{k-1}^{Tr}}{\cos\theta_{k-1}^{Tr}} & \dfrac{\cos\phi_{k-1}^{Tr}}{\cos\theta_{k-1}^{Tr}} \end{bmatrix} \tag{4.3.2}$$

The quantity $\vec{\omega}_{Tr/NED,k-1}^{Tr}$ is the IMU measured trunk angular rate with Earth Rate removed as described in [11] .

For the pedestrian navigation application the transport rate of the angular rate can be neglected since the maximum velocity is around 2 m/s. This translates to a transport rate on the order of $10^{-5}\,^{\circ}/s$ which is negligible when compared to the IMU noise shown in **Table 1** and discussed later in the paper.

After each IMU measurement is processed, the condition to declare the end of the stride is checked. The end of a stride is declared if the following three conditions are satisfied: The foot mounted INS system declares a ZUPT measurement is valid; it has been longer than 0.4 seconds since the foot mounted EKF system processed a ZUPT measurement; and if the difference between the position solution calculated at the previous ZUPT and the current position is greater than $0.2m$. If these conditions are satisfied the, the *a*

priori orientation of the trunk at the end of the current stride is set to the quantity that has been computed using the IMU update as shown in Equation (2). That is,

$$\left[\phi_s^{Tr-}, \theta_s^{Tr-}, \psi_s^{Tr-}\right]^T = \left[\phi_k^{Tr}, \theta_k^{Tr}, \psi_k^{Tr}\right]^T \tag{4.3.3}$$

If a turn is detected the *a priori* estimate of the attitude becomes the *a posteriori* estimate used to initialize integration of the gyroscopes for the next stride. This effectively makes the system run without measurement updates until the next straight line walking stride is detected. If no turn has been detected the trunk attitude of the previous stride is used to compute the *a posteriori* attitude as the sum of the *a priori* attitude estimate and a portion of the bias that is dependent on s_s, which is the number of straight strides that have been detected at the current measurement update. That is,

$$\begin{bmatrix} \phi_s^{Tr+} \\ \theta_s^{Tr+} \\ \psi_s^{Tr+} \end{bmatrix} = \begin{bmatrix} \phi_s^{Tr-} \\ \theta_s^{Tr-} \\ \psi_s^{Tr-} \end{bmatrix} + K\left(\frac{1}{s_s}\sum_{i=2}^{s_s}\left(\begin{bmatrix} \phi_{i-1}^{Tr+} \\ \theta_{i-1}^{Tr+} \\ \psi_{i-1}^{Tr+} \end{bmatrix} - \begin{bmatrix} \phi_i^{Tr-} \\ \theta_i^{Tr-} \\ \psi_i^{Tr-} \end{bmatrix}\right)\right) \tag{4.3.4}$$

The gain K determines how much feedback should be applied to the system. If $K = I_{3x3}$ (the identity matrix), the system would apply all of the average bias to the current stride making the attitude equal to the attitude of the trunk at the previous stride end plus an angle bias term that comes from the averaged angle difference over all straight strides through the current stride. If the gain is zero, no feedback is applied to the system and open loop integration occurs.

For the validation experiments described later in the paper, a K matrix that was calculated in the following manner was used: It is based on the measured deviations of the variation in attitude parameters over strides determined to be straight line motion. That is,

$$K = \begin{bmatrix} \dfrac{\sigma_{\text{ol}}^2}{\sigma_{\text{ol}}^2 + \sigma_{\sum \Delta\phi_s}^2} & 0 & 0 \\ 0 & \dfrac{\sigma_{\text{ol}}^2}{\sigma_{\text{ol}}^2 + \sigma_{\sum \Delta\theta_s}^2} & 0 \\ 0 & 0 & \dfrac{\sigma_{\text{ol}}^2}{\sigma_{\text{ol}}^2 + \sigma_{\sum \Delta\psi_s}^2} \end{bmatrix} \tag{4.3.5}$$

where σ_{ol}^2 is the square of the open loop error accumulated over an average period of time without measurement updates computed using Equation (4.3.6). Mathematically, this is given as

$$\sigma_{\text{ol}}^2 = (n\sigma_{\mu g}\Delta t_{stride})^2 + n(\sigma_{wg}\Delta t_{stride})^2 \tag{4.3.6}$$

where *n* is the number of strides since the last attitude update, $\sigma_{\mu g}$ is the gyro bias which is assumed to be fully correlated over the strides and σ_{wg} is the wide band noise of the gyro which is assumed to be uncorrelated between individual strides. The quantities $\sigma^2_{\sum \Delta\phi_s}$, $\sigma^2_{\sum \Delta\theta_s}$, and $\sigma^2_{\sum \Delta\psi_s}$ are the square of the standard deviations of average roll, average pitch and average yaw differences over a stride.

$$\sigma_{\sum \Delta\psi_s} = \mu_{\Delta\psi_s} + \frac{1.2}{\sqrt{s_s}}\sigma_{\Delta\psi_s} \tag{4.3.7}$$

The quantity $\mu_{\Delta\psi_s}$ is the mean of the yaw parameter, $\sigma_{\Delta\psi_s}$ is the standard deviation of the yaw parameter determined from the set of data compiled in **Table 3** (which, in turn, is determined from the baseline statistics of trunk roll and yaw changes in Figures 6 and 7), and s_s is the number of straight strides that have been detected at the current measurement update. The 1.2 is an inflation factor applied due to the distribution of the yaw angle change over a stride being non-Gaussian as shown in Figure 2-1. Both the average pitch and average roll standard deviations are computed using equation (4.3.7) with the mean and standard deviation quantities from **Table 3**.

5 Algorithm Validation Results

This chapter describes the results of differencing the navigation parameters computed by the preceding algorithms from IMU data with the Vicon™ derived navigation quantities. The comparison allows for assessment of the performance of the navigation algorithms since the Vicon™ system supplies an accurate, independent, and more direct measure of the navigation quantities of interest.

5.1 TRUNK ATTITUDE DRIFT REDUCTION

In assessing the performance of the algorithm developed in this paper, the first thing we need to do is to verify whether the assumption about the variations of $\Delta\psi_T$ and $\Delta\phi_T$ during straight line walking is valid. **Table 3** provides a summary of the statistics for these and other relevant parameters. Note that the mean and standard deviation of the trunk roll parameter are lower than the mean and standard deviation of the trunk

yaw parameter. We believe that this makes intuitive sense because the trunk of a person is free to rotate about the yaw axis and still be able to follow the bulk motion of the trajectory. On the other hand, if the trunk were to consistently have a mean roll angle change over stride the person would fall to the ground due to the effects gravity has on a person's trunk with a large roll angle.

Another critical piece of data in ***Table 3*** is that the gyro sum standard deviation over stride. This is the amount of error that is expected if integration of the gyroscopes is relied on to track attitude. This number is equal to 0.47°, which is less than the trunk yaw change mean, trunk roll change mean, and trunk pitch change mean over the stride. This implies that the error expected to accumulate from relying on the constraint that the orientation has not changed over strides determined to be straight is less than the error expected from relying on open loop integration of the IMU's gyroscopes for attitude.

Table 3 The Statistics of the Change in Trunk Angles Over a Stride

Parameter	Value
Trunk Yaw Change Mean	-0.17 °
Trunk Yaw Change Stdv	1.73°
Trunk Roll Change Mean	0.06°
Trunk Roll Change Stdv	1.37°
Trunk Pitch Change Mean	0.11°
Trunk Pitch Change Stdv	1.25°
Gyro Sum Stdv Over Stride	0.47°

For all runs that contained trunk Vicon data, trunk IMU data, and foot IMU data the trunk attitude determination algorithm was run using the IMU and compared to the orientation produced by the Vicon system. The key metric for the runs is percent yaw error reduction at the end of the run which is computed as the yaw error of the open loop minus the yaw error computed using the method defined in the paper all

divided by the yaw error of the open loop. This is then multiplied by 100 to get a percent value. **Table 4** shows that the majority of the runs are improved by applying the presented algorithm. However there are some runs where the improvement is not statistically significant. This is because the rate of heading change in some of the trajectories was smaller than the error expected due to gyro drift.

Table 4 The average trunk yaw angle error reduction at the end of run by participant

Participant	Number of runs with all data present	Average % Trunk Yaw Angle Error Reduction at End of Run
2	2	25%
4	1	6%
5	2	55%
6	1	2%
8	3	63%

Figure 5-1 shows the path of the right foot measured by the foot mounted ankle dot traveled by subject 8 during trial 5 (refered to as trial 805). This particular trajectory is representative of those trajectories that showed improvement in yaw error reduction through applying the trunk attitude constraint. Minimal out of plane motion is present during the straight segments and the turn segments are very compact.

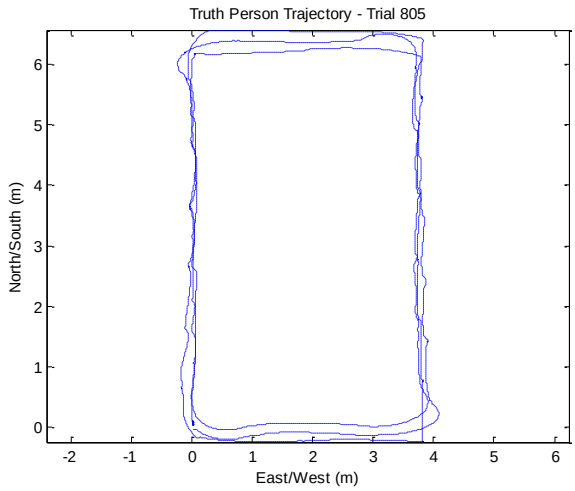

Figure 5-1 The true path of the foot traveled during a trajectory where heading accuracy was significantly increased by applying trunk attitude constraints

Figure 5-2 shows the improvement made for the subject eight walking the trajectory shown in Figure 5-1. Note that any areas of the plot shaded in grey are where the Vicon system was marked unhealthy. At the end of the run the error in the unaided or open loop case shown in blue is around 12°, but the error in the aided case using trunk roll, pitch and yaw constraints is 4° for a 66% yaw error reduction. The manner in which the drift decrease is important to observe as well. In the beginning of the run additional error was produced by the algorithm since the first few strides appear to be curving motion, but by the end of the run the rate of change of the yaw error is very low meaning that the algorithm has successfully been able to estimate the bias of the gyroscopes that combined integrate into the yaw axis error (note that in this case that was almost exclusively the z-axis gyro due to the trunk IMU mounting configuration show in *Figure 3-7*)

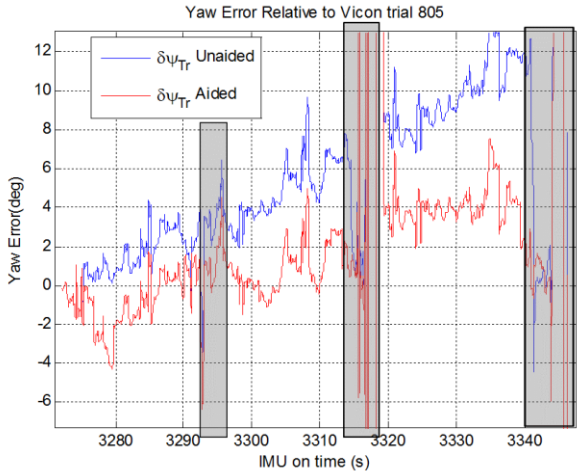

Figure 5-2 The comparison of trunk attitude error relative to the Vicon reference system

The change in trunk yaw against the stride number is shown in Figure 5-3, the raw trunk yaw change over a stride is plotted in blue and the moving average of trunk yaw change over stride is plotted in green. This plot

shows that although on a stride to stride basis there is significant variation the mean value of the deviation over the stride settles to the low frequency component caused by the gyroscope drift. This is the parameter that is then multiplied by the gain plotted in Figure 5-4 and then fed back to correct the attitude in equation (4.3.4).

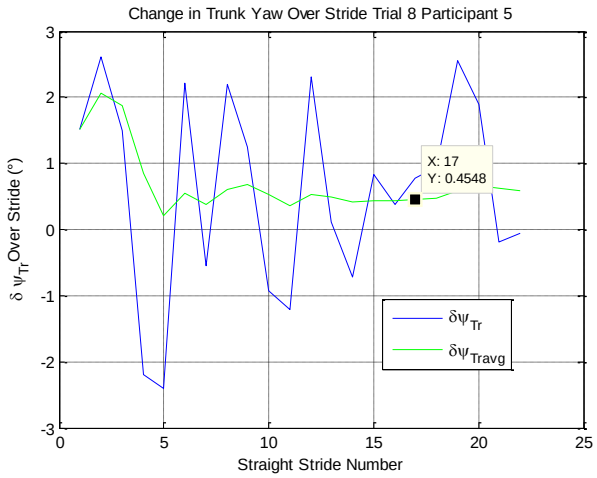

Figure 5-3 The change in trunk yaw over strides vs. stride number

In *Figure 5-4* we plot the gain for this feedback during trial 805. This plot illustrates that the gain is low initially due to the low number of measurements of change in trunk attitude over stride. As the number of attitude measurements increases the gain increases since the mean of the change in trunk yaw is known better due to more samples to observe the straight line motion. Notice however that as the number of strides increases the gain will reach a steady state value that is not one since there is some uncertainty that the trajectory of the person is actually a straight line. The uncertainty of linear motion for a person is determined in this experiment to be the mean of the full set of yaw data collected in Table **3**. In effect this is adding process noise in the trunk attitude filter systems which add additional uncertainty to the ability of the estimator to retain information about the direction of travel.

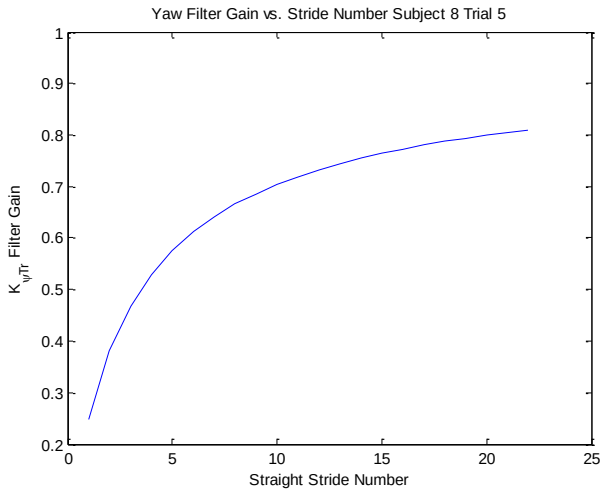

Figure 5-4 The filter gain as a function of stride number for trial 805

As shown in **Table 4** there were a number of runs where performance was not able to be significantly improved. These runs were all very similar to trial 205 which has a path shown in Figure 5-5. Compared to the trajectory measured in by trial 805 shown in Figure 5-1 both the North/East and South/West directions of travel were shorter by about 2 m or about 1 stride each. Also, the trajectory was more curved in nature than the trajectory ground track taken by the participant in trial 805. These factors contributed to less straight line motion segments and limited the amount of data available to measure average attitude deviation caused by the gyroscopes over strides.

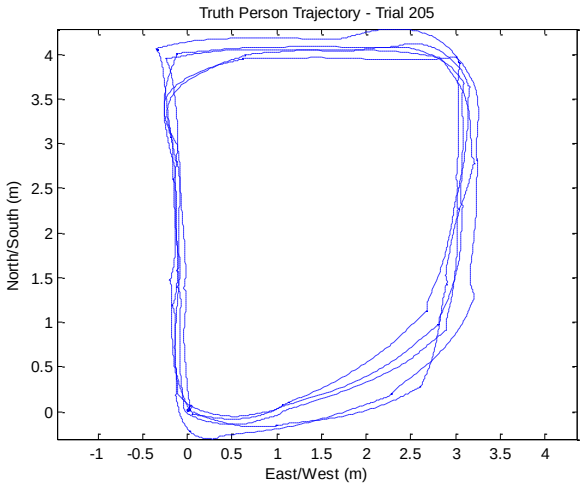

Figure 5-5 The path of a run where the heading error reduction method was ineffective

Figure 5-6 shows the time history of the yaw angle error for the unaided open loop integration in blue and the trunk attitude constraint method of aided closed loop in red. This particular trial had a combination of very limited number of straight line segments which is evident by the closeness of the red and blue curves in

the figure. Also evident in *Figure 5-6* is some periods of time where real trunk yaw motion is removed by the attitude filter and added back between the time into run of 25-33 seconds. The error in the attitude initially decreases suddenly at 25 seconds in and then comes back at 33 seconds in. This is an example of where real motion is eliminated by the hard cutoffs of the algorithm at 3.5° of yaw deviation over the stride.

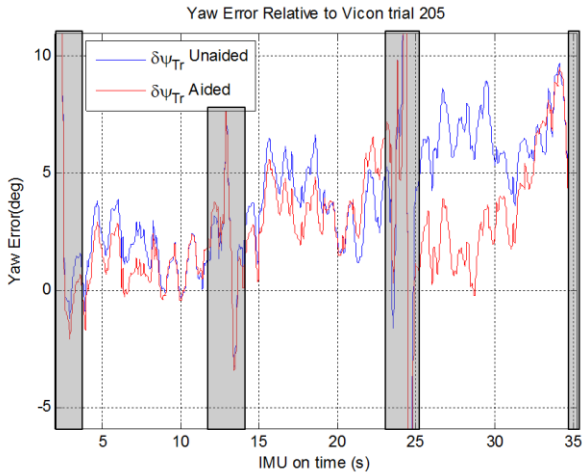

Figure 5-6 The yaw error for trial 205 which is a trial with limited performance improvement from the trunk attitude constraint algorithm

5.2 FOOT MOUNTED SUB-SYSTEM NAVIGATION RESULTS

The foot mounted sub-system is used to determine the attitude measurement start and end points, stride width, and change in foot yaw over a stride that are used in the turn determination algorithm described in section 4.2. The foot mounted method of personal navigation is also a commonly used tactic to reduce the drift of pedestrian navigation inertial navigation algorithms.

5.2.1 Open Loop Navigation – Vicon Derived Inertial Data

In order to check that the open loop integration algorithms are working the Vicon derived inertial data created by the methods described in section 3.3.3 is passed through the open loop inertial navigation algorithms described in section 4.1.2. Since the Vicon derived inertial data does not have the measurement errors present in the IMU data any difference between the integration of the Vicon derived inertial data and the Vicon position must be due to integration algorithm errors. The blue trace in *Figure 5-7* shows the North, East, Down position error vs. time and the black traces show the standard deviation of navigation with an IMU with error characteristics shown in **Table 1**. Since the absolute value of the blue trace is so much smaller than the black traces the algorithmic error is sufficient to perform navigation with the IMUs used for this experiment. This is especially evident in the velocity difference between the navigation algorithms and the Vicon velocity shown in *Figure 5-8*.

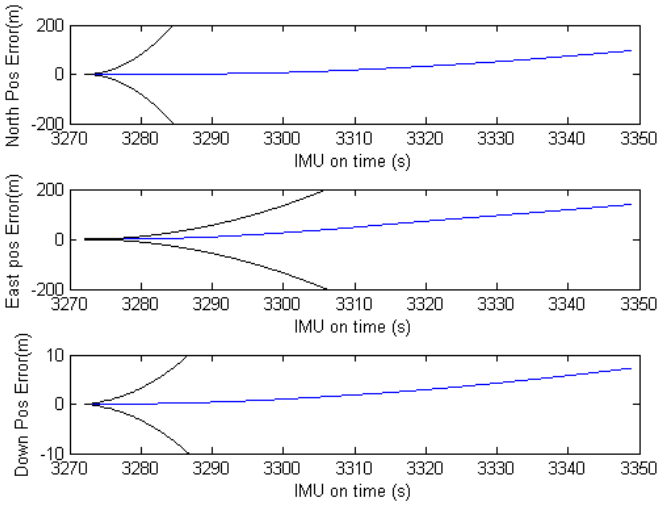

Figure 5-7 The difference between the integration of Vicon derived inertial data and Vicon position measurements

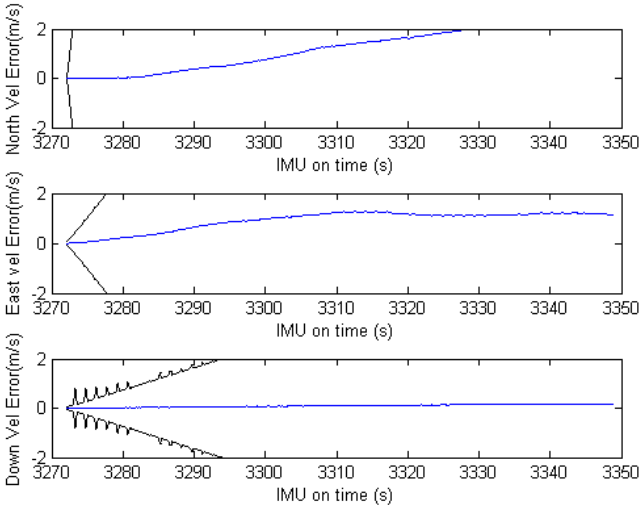

Figure 5-8 The velocity difference between the open loop integrated Vicon derived inertial data and Vicon velocity

5.2.2 Closed Loop Navigation – Vicon Derived Inertial Data

To make sure the closed loop navigation algorithms work as expected the algorithms are tested with the Vicon derived inertial data. *Figure 5-9* shows the closed loop velocity vs. time in the North (blue), East (green) and Down (red) traces. The black dots indicate points where ZUPTs are declared valid. This figure shows that as the navigation velocities go to zero during the stance phase the ZUPT updates are declared valid.

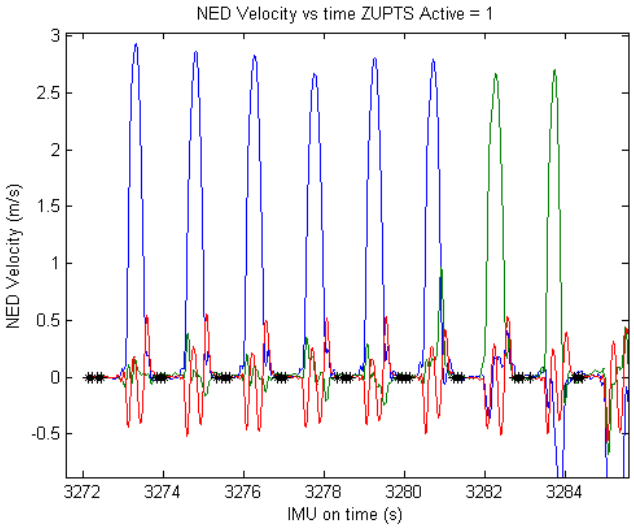

Figure 5-9 The NED velocity vs. time

Figure 5-10 shows the position error vs. time for the integrated Vicon derived inertial data with ZUPTs active. This plot shows that the position error drift is very minimal and is in line with the value the covariance predict (black trace) with the exception of the vertical axis where the gravity instability limits the accuracy of the solution.

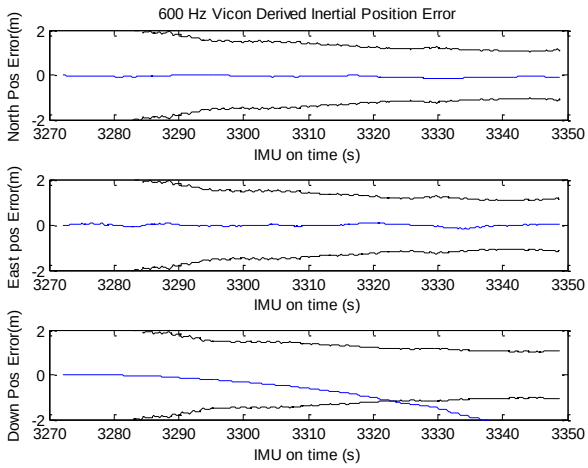

Figure 5-10 The NED position error vs. time for ZUPT closed loop navigation with Vicon derived inertial data

Figure 5-11 shows the velocity error vs. time in each of the NED axes. As expected the velocity errors are minimal due to the zero velocity resets. The standard deviation values stay fairly small due to the constant measurements provided by the zero velocity conditions.

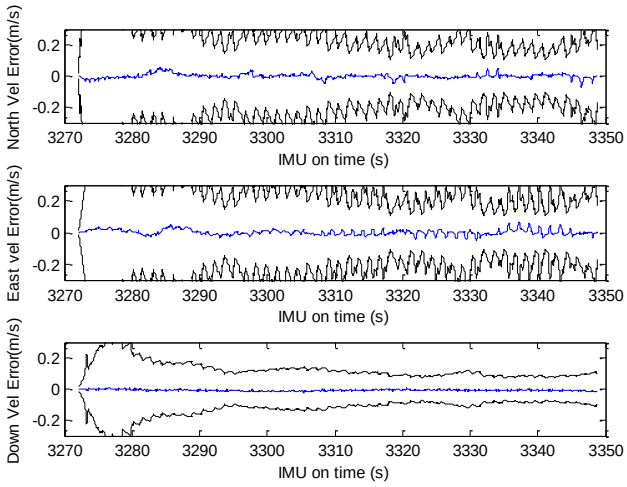

Figure 5-11 The velocity error vs. time

Figure 5-12 shows the attitude error vs. time for the ZUPT closed loop Vicon derived inertial navigation. As expected the covariance values of the roll and pitch quantities do no grow with time since the ZUPT measurements allow for observation of these quantities but the yaw covariance does not decrease since ZUPTs do not observe the yaw quantity.

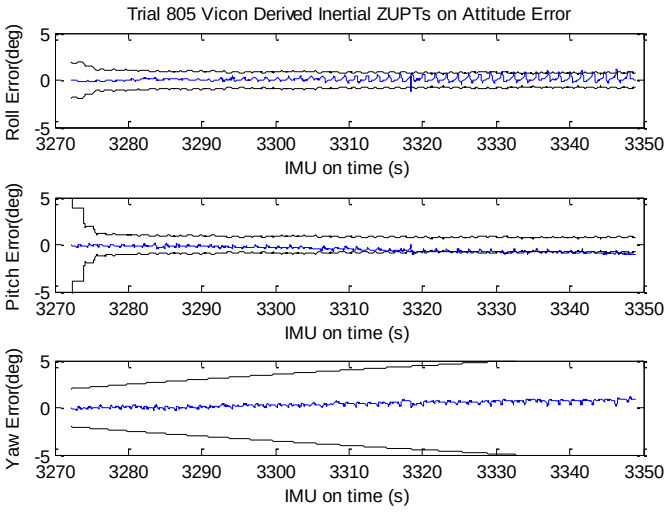

Figure 5-12 The attitude error vs. time

5.2.3 Closed Loop Navigation ZUPT Measurements – IMU Inertial Data

The only difference between running the algorithms using the Vicon derived inertial data and the IMU is the additional errors present in the measurements of acceleration and angular rate. *Figure 5-13* and *Figure 5-14* show that the position error vs. time is very similar to navigation with the Vicon derived inertial up until the point around 3315 seconds into the run where the heading error exceeds the standard deviation and

the position error has a component of error that is significant in the axis perpendicular to the direction of travel that builds over time as the steps are projected in the incorrect direction.

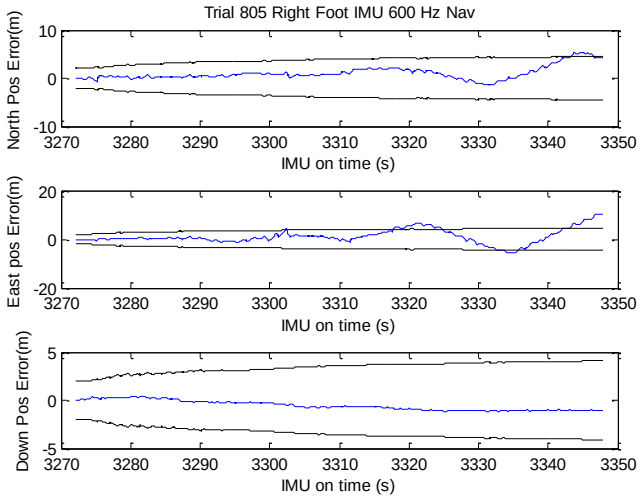

Figure 5-13 The position error vs. time for navigation with the IMU at 600 Hz iteration rate

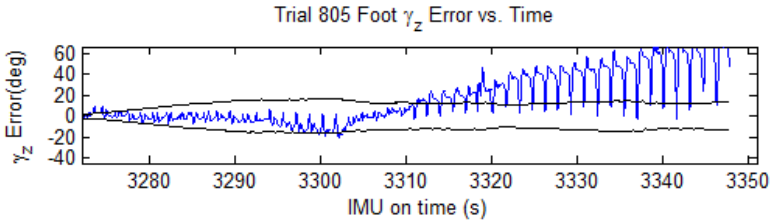

Figure 5-14 The heading error vs. time for IMU navigation of the foot

6 Conclusions and Future Work

In this thesis a method of reducing the heading error drift for pedestrian navigation was developed and validated using data from eight healthy individuals walking paths similar to typical paths encountered in confined indoor spaces. The average change in trunk roll, pitch, and yaw angle over stride across all 8 subjects was shown to be zero mean to within the repeatability of the integrated gyroscope turn on to turn on bias for strides determined to be straight line motion. This is a significant finding since it shows that pedestrian turn detection leads to precise enough information to be used in attitude aiding of a trunk mounted IMU.

The heading error relative to Vicon® reference results showed that the algorithm significantly reduced the errors in heading drift relative to simple open loop gyroscope integration for six out of nine trials and minimally reduced the errors for the other three trials. These results indicate that the method of heading drift reduction developed in this thesis is a candidate to augment a pedestrian navigation system.

The method of heading drift reduction is based on the heuristic constraint that in indoor environments individuals tend to walk along straight line paths since buildings are generally constructed as series of straight corridors. The paths traveled by the participants in the experiments used to validate the experiment are the most confined paths for potential application of indoor navigation and the method of reducing the yaw error still reduced the yaw error an average of 40% relative to open loop yaw determination using gyroscope integration alone for nine paths walked by six different subjects. The confined nature of the environment used is due to the restrictions imposed by the Vicon® measurement system and represents one of the smallest paths where this measurement assumption can be used.

The experiment developed in this work made use of an established method of tracking motion indoors for comparison to the experimental algorithms developed in this work to aid heading estimation for a trunk mounted attitude reference system. This experiment incorporated many novel techniques to align the Vicon and IMU measurements in time and coordinate space resulting in a unique data set to evaluate personal navigation algorithms under the trajectory restrictions of the experiment.

Future work

Perform integrated INS/Vicon Navigation system to eliminate turn on to turn on repeatability impact on turning results. Since the Vicon data alone has dropout issues during turns the IMU would complement the Vicon during turning segments and determine the limits of mean motion more accurately. The outcome of the integration would also compute trunk gyro bias values which could be compared to the value predicted by the drift reduction method.

The method of reducing the yaw gyroscope drift of the trunk mounted attitude heading reference system is based solely on difference in attitude between the initial contact point of the foot to the ground at the current stride and the previous stride since each foot contact point is at a common location in the periodic motion of the upper torso. Comparing more points in the periodic motion may provide extra information about the trajectory being traveled and the gyroscope drift errors.

The nature of the experiment constrained the trajectories to a small path that is much more confined than the typical indoor navigation environment. This leads to very few straight strides to observe the drift in the z-trunk gyroscope, potentially leading to lower performance than in a less confined navigation environment. Any future experiment performed should be conducted in a less confined space more representative of buildings where navigation information is desired.

The data collected from the experiment described in this thesis is useful for comparison of Navigation algorithms to a known truth. This can serve as a generic platform to evaluate Personal Navigation algorithms on different body parts. The general methods presented for combined processing of Vicon and IMU data can be used for working toward elimination of 'data set' or trajectory ambiguity in personal navigation papers.

7 References

[1] A. Jimenez Ruiz, F. Seco Granja, J. Prieto Honorato, and J. Guevara Rosas. "Accurate pedestrian indoor navigation by tightly coupling foot-mounted IMU and RFID measurements." *IEEE Transactions on Instrumentation and Measurement* (2012): 178-179. Web.

[2] Alvarez, Juan C., et al. "Pedestrian Navigation Based on a Waist-Worn Inertial Sensor." *Sensors* (2012). Web.

[3] Bornstein, J, L Ojeda and S and Kwanmuang. "Heuristic Reduction of Gyro Drift." *Journal of Navigation* (2009): 41-58. Web.

[4] Cho, Seong Y., and Chan G. Park. "MEMS Based Pedestrian Navigation System." *Journal of Navigation* (2006): 135-153.

[5] Craig, John J. *Introduction to Robotics Mechanics and Control*. Upper Saddle River, NJ: Pearson/Prentice Hall, 2005. Print.

[6] Foxlin, Eric. "Pedestrian Tracking with Shoe-mounted Inertial Sensors." Computer Graphics and Applications." *IEEE* (2005): 38-46. Web.

[7] Gebre-Egziabher, Demoz. *gnss_ins_EKF_PA_Cbn*. Minneapolis, 2012. Matlab Code.

[8] Gleason, Scott and Demoz Gebre-Egziabher. *GNSS Applications and Methods*. Boston: Artitech House, 2009. Web.

[9] Groves, Paul D. *Principles of GNSS, Inertial, and Multi-sensor Integrated Navigation Systems*. Boston: Artech House, 2008. Print.

[10] Hase, K. and Stein, B. "Turning Strategies During Human Walking." *The American Physiological Society* (1999): 2914-2921. Web.

[11] Jakel, Thomas and Demoz Gebre Egziabher. "Use of Trunk Roll Constraint to Improve Heading Estimation in Pedestrian Dead Reckoning Navigation Systems." Proceedings of ION GNSS+. Nashville, 2013.

[12] Kirker, Ryan M. *Stride Length Determination Based on a Single Axis Accelerometer Measurement and a Kinetic Model for Human Gait*. Master's Thesis. Minneapolis, 2012. Print.

[13] M. Susi, D. Borio, and G. Lachapelle. "Accelerometer signal features and classification algorithms for positioning applications." *Procedings of the 2011 Int. Technical Meeting of The Institute of Navigation* (2011). Web.

[14] Mathworks. *SVD - Singular Value Decomposition*. n.d. Software. 12 December 2012.

[15] Matthews, Christopher J. "In-Situ Stride Length Estimation Using a Kinetic Model of Human Gait." Master's Thesis. 2011. Print.

[16] Panahandeh, Ghazaleh, et al. "Continuous Hidden Markov Model for Pedestrian Activity Classification and Gait Analysis." *Instrumentation and Measurement* (2013): TBD. Web.

[17] Patla, A.E., A Adkin and T. and Ballard. "Online Steering: Coordination and Control of Body Center of Mass, Head and Body Reorientation." *Experimental Brain Research* (1999): 629-634. Web.

[18] Patla, A.E., et al. "Visual Control of Locomotion: Strategies for Changing Direction and for Going over Obstacles." *Journal of Experimental Psychology: Human Perception and Performance* (1991): 603-634. Print.

[19] Rozumalski, Adam. *Gillette Children's Hospital Vicon Motion Capture System Accuracy* Thomas Jakel. 27 July 2012.

[20] Simon, Dan. *Optimal State Estimation: Kalman, H_infinity, and Nonlinear Approaches*. Hoboken: Wiley, 2006. Print.

[21] Veth, Mike, and John Raquet. "Fusion of Low-Cost Imagining and Inertial Sensors for Navigation." *Proceedings of the 19th International Technical Meeting of the Satellite Division of The Institute of Navigation* (2006): 1093-1103. Web.

[22] Wan, Sheng and Eric and Foxlin. "Improved Pedestrian Navigation Based on Drift-Reduced MEMS IMU Chip." *Procedings of the 2010 International Technical Meeting of The Instititute of Navigation* (2010): 220-229. Web.

8 Appendix

8.1 EXPERIMENT NOTES

Analysis of Human Gait during Turning Motion

Experiment Set Up

Experiment Equipment:

6 Bluetooth Wireless Inertial Measurement Units (IMUs)

Computer or wireless device with Bluetooth logging software for IMUs

Charging stations or cords for wireless IMUs

Velcro mounting straps for IMUs

Flat surface for IMU start-up

Vicon Motion Capture System including markers and data logging computer

Flat open floor space within range of Vicon Motion capture system

Procedure:

Place the 6 fully charged wireless IMUs on a flat surface

Open the Bluetooth IMU V2 Multi-Logger on the IMU logging computer

Turn the IMUs on by toggling the on switch after which a green light should flash on each IMU

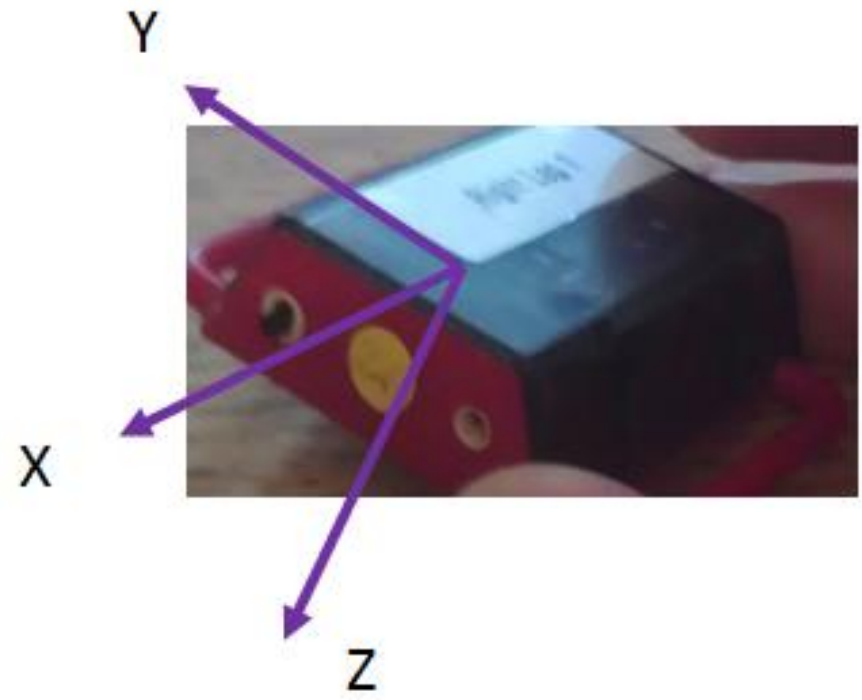

From the Bluetooth IMU Logger select the Connect All button

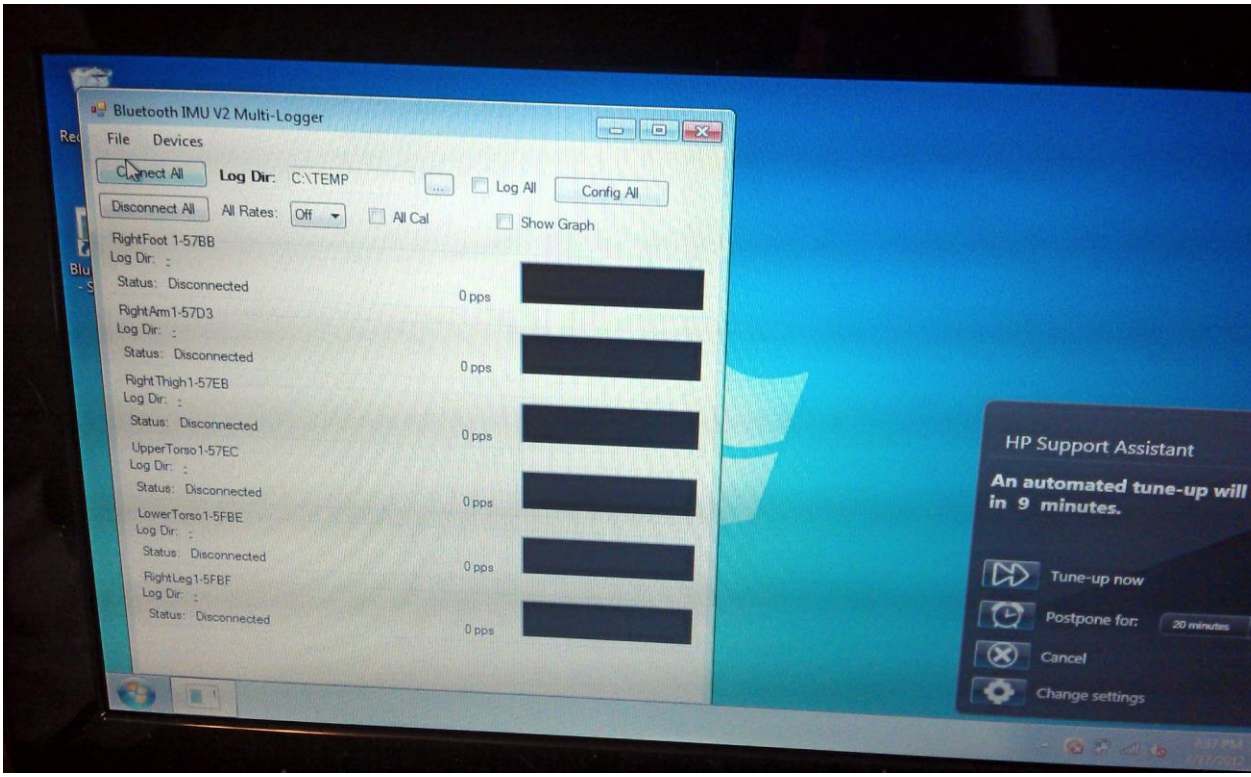

Wait for a successful connection indicated by a blue light on the IMU and a status of Connected! on the logger screen

Once the IMU is connected select 100 under the All Rates pull down menu

Select the Config All button in the upper right corner of the Bluetooth IMU Logger Screen

Wait for the Status of the IMU to go to Configuration Sent!

Select the desired log directory for the IMU data - Name the end folder with subject number and the label Initial_Calibration

Check the Log All radial button

Log data for approximately 60 seconds

Uncheck the Log All radial button

Attach the right foot IMU (labeled Right Foot) as shown in Figure IMU (6)

Attach the right ankle IMU (labeled Right Leg 1) as shown in Figure IMU (5)

Attach the right thigh IMU (labeled Right Thigh) as shown in Figure IMU (4)

Attach the lower torso IMU (labeled Lower Torso 1) as shown in Figure IMU (3)

Attach the right arm IMU (labeled Right Arm 1) as shown in Figure IMU (2)

Attach the upper torso IMU (labeled Upper Torso 1) as shown in Figure IMU (1)

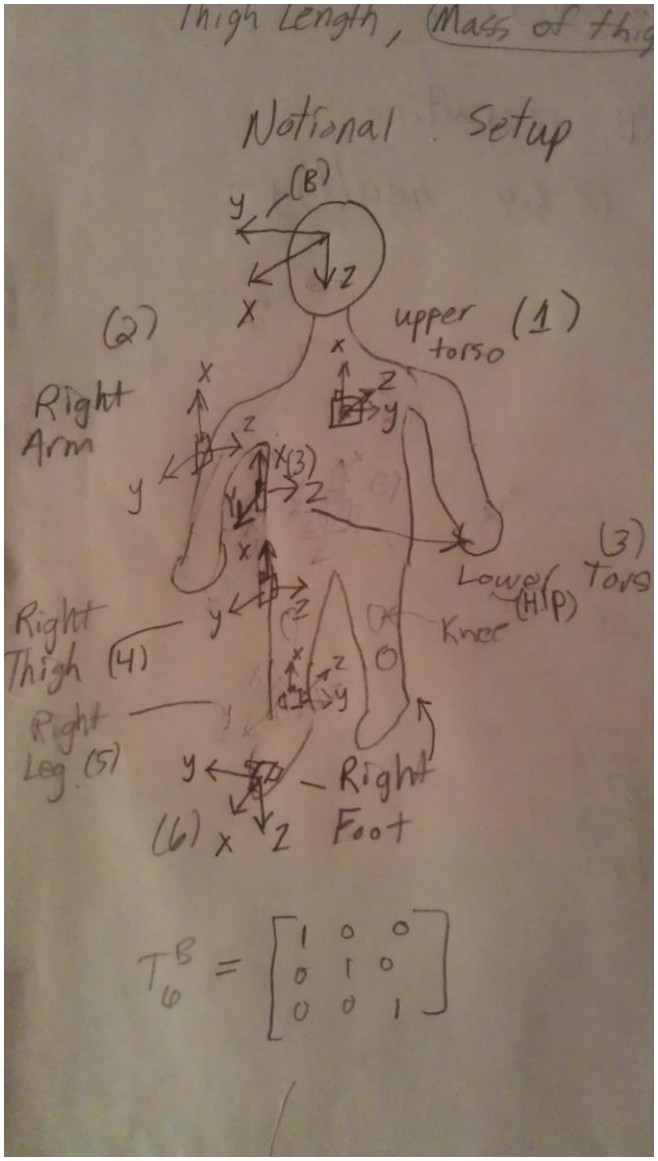

Figure 4. The Mounting Orientation of IMUs on the participant (1) Upper Torso IMU (2) Right Arm IMU (3) Lower Torso IMU (4) Right Thigh IMU (5) Right Leg IMU (6) Right Foot IMU

[Physical Therapist] Attach the standard set of markers for tracking lower body and torso motion tracking

[Physical Therapist] Place markers just above and below two diagonal corners of each IMU

Trial Portion

Have the subject move to a side of the Vicon tracking area

Once all of the markers are active begin logging Vicon data and IMU Data by checking the Log All button - make sure the file is named descriptively with the subject number and the type of trial being done

Have the subject jump in the air to begin the trial portion of the experiment

Have the subject remain as still as possible for a 5 second period

Dynamic Trial Portion

Have the subject walk back and forth in a straight line at a normal walking pace to the end of the Vicon Tracking area and back to the starting point 10 times

Repeat steps 20-23.

10. Collect 3 turning trials of 10 circles of the testing area per trial with the participant making a 45° degree turn in the middle of the testing area

a. Trial 1 – Slow Walking

b. Trial 2 – Free Speed Walking

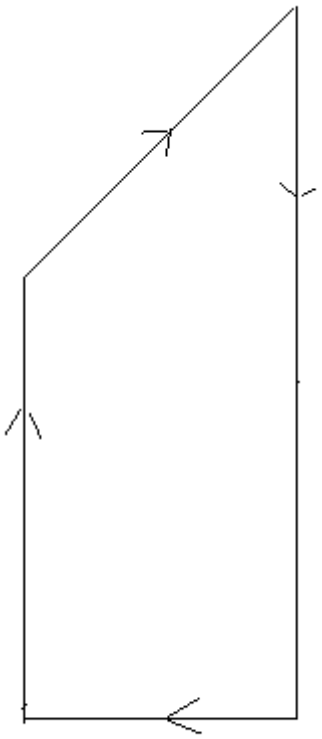

c. Trial 3 – Fast Speed Walking

Repeat steps 20-23.

11. Collect 3 of turning trials of 10 circles of the testing area per trial with the participant making a 90° degree turn near the end of the testing area

a. Trial 1 – Slow Walking

b. Trial 2 – Free Speed Walking

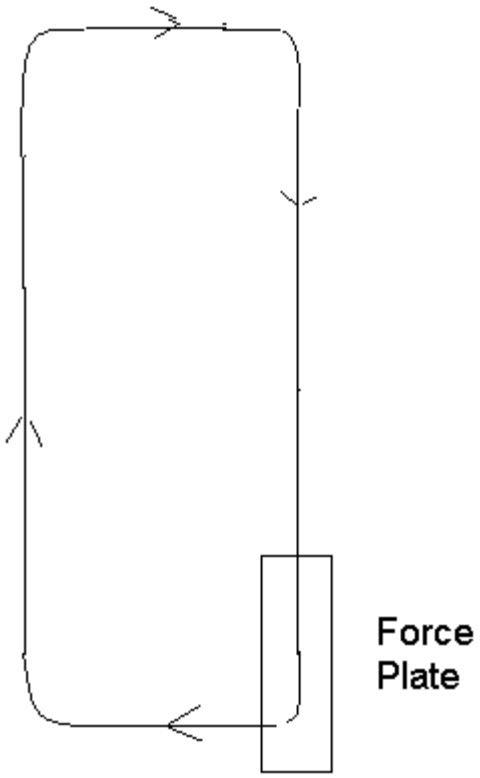

c. Trial 3 – Fast Speed Walking

Repeat steps 20-23.

12. Collect 3 of turning trials with the participant performing 10 s-turns (one turn is pictured and the end of each sequence the participant will stop, turn around and repeat)

a. Trial 1 – Slow Walking

b. Trial 2 – Free Speed Walking

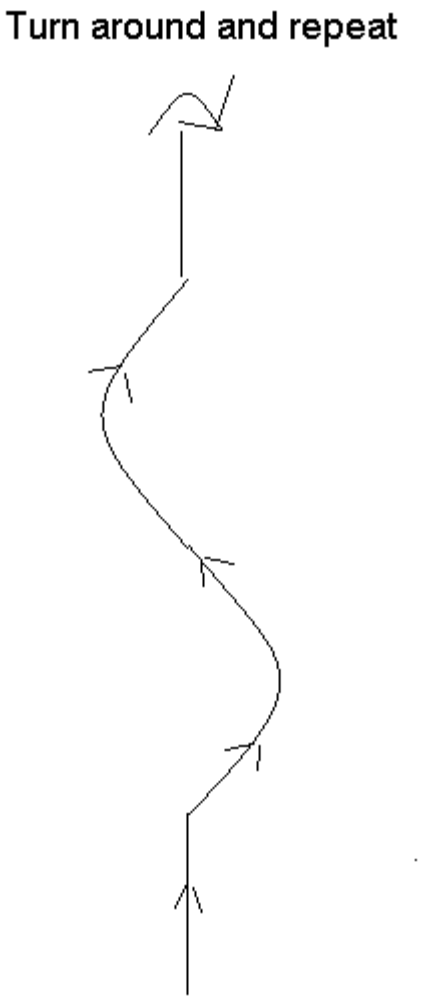

c. Trial 3 – Fast Speed Walking

[Technician] Back up data

8.2 MATLAB CODE

The Matlab code and data is available upon request. Please e-mail me at jake0013@umn.edu or jake006725@gmail.com to request the code.